UNIVERSITÀ DEGLI STUDI DI PADOVA
DIPARTIMENTO DI INGEGNERIA INDUSTRIALE

Tesi di Laurea Magistrale
in Ingegneria dell'Energia Elettrica

Operation optimization of a multi-energy microgrid under uncertainties

Relatore: Prof. Roberto Turri
Correlatore: Dr. Cuo Zhang

Pierpaolo Garavaso
Matricola 1179264

Aprile 2020

Anno Accademico 2019/2020

“To me, it underscores our responsibility
to deal more kindly with one another,
and to preserve and cherish the
pale blue dot, the only home
we've ever known.”
Carl Sagan

TABLE OF CONTENTS

ABSTRACT

Multi-energy microgrids (MEMG) can simultaneously distribute and supply electrical and thermal energy to customers. By coupling together electrical and thermal networks, traditionally independently operated, system operators can benefit from higher flexibility while also allowing the integration of distributed generators. However, MEMGs operation is strongly affected by uncertain parameters, such as renewable sources output, electric loads and temperature-dependent thermal loads, which can never be perfectly forecasted. If not adequately modelled, the uncertainty related to these parameters may deviate the economic and feasible dispatch from its optimal value. This thesis work proposes a coordinated dispatch method to minimize the operating costs of a MEMG when multiple uncertain parameters are considered.

First, the system model was built considering devices and network constraints. Then, the operation method was modeled as a single-stage stochastic programming problem. To capture uncertainty variability, Monte Carlo sampling technique was used to generate a large number of random scenarios. Sets with different numbers of representative scenarios were selected, generating uncertainty models with different accuracy levels and computational burdens. The proposed stochastic operation method was tested on a 14-bus system to find the optimal day-ahead operation dispatch. After that, a feasibility check was carried out based on a set of new scenarios and the corresponding solutions were compared. The results demonstrated that the proposed operation model can achieve robust solutions when uncertainties are accurately modeled and, therefore, can be properly used for day-ahead operation planning.

RIASSUNTO

Le microreti multienergetiche (MEMG) sono dei sistemi in cui le reti di distribuzione elettrica e termica sono accoppiate l'una all'altra da componenti le cui dinamiche influenzano entrambi i sistemi. Compito del gestore della MEMG è quindi quello di garantire l'approvvigionamento dei carichi elettrici e termici della rete rispettando contemporaneamente i vincoli d'esercizio di entrambi i sistemi di distribuzione. Sebbene la gestione di un tale sistema sia più complessa rispetto a quella dei singoli sistemi, le MEMG permettono una gestione più flessibile ed uno uso più efficiente delle fonti a disposizione. In particolare, in una MEMG ad elevata penetrazione di fonti rinnovabili, l'accoppiamento dei sistemi elettrico e termico è un metodo efficace per meglio gestire la loro aleatorietà e contemporaneamente massimizzare il loro utilizzo.

Oltre a numerosi vantaggi, le MEMG portano con sé, tuttavia, anche le criticità dei singoli sistemi. In particolare, sistemi di questo tipo sono fortemente influenzati dall'incertezza dei parametri del modello di rete. Per questo motivo, se le incertezze che influenzano il sistema non vengono adeguatamente modellate, la pianificazione del dispacciamento può risultare molto lontana dal suo ottimo, sia in termini di costo di esercizio che di sostenibilità della rete. Per gestire tale problema, in questo lavoro di tesi è stato realizzato un modello in ambiente MATLAB per il dispacciamento di una MEMG capace di garantire una soluzione ottima quando diverse fonti di incertezza perturbano il sistema.

Per prima cosa si è costruito il modello della MEMG definendo i vincoli di funzionamento dei componenti e delle reti di distribuzione sia elettrica che termica. Successivamente, il modello di gestione è stato formulato come un problema di programmazione stocastica lineare a singolo stadio. Si osservi che è stato possibile adoperare questo metodo solo grazie all'ipotesi di conoscere le funzioni di distribuzione di probabilità delle incertezze analizzate, che in questo modello si suppongono avere distribuzione normale. Sfruttando quindi la tecnica di campionamento casuale di "Monte Carlo" si è generato un vasto numero di possibili scenari, ovvero possibili valori che i parametri incerti potrebbero assumere. Si è poi ridotto il numero iniziale di scenari usando il metodo di "Riduzione simultanea all'indietro" (*simultaneous backward reduction*, in inglese) in modo da ottenere dei modelli di incertezze meno computazionalmente onerosi da usare durante le simulazioni. Dal momento che il numero di scenari a cui si riduce l'insieme iniziale generato da Monte Carlo è proporzionale all'accuratezza con cui l'incertezza verrà modellizzata, maggiore è il numero e maggiore saranno sia l'accuratezza che l'onere computazionale.

Il modello di gestione così costruito è stato testato su una rete elettrica e termica a 14 nodi e i valori delle variabili di controllo sono stati confrontati con la soluzione deterministica del dispacciamento, ovvero quella non considera le incertezze. I risultati hanno dimostrato che il costo d'esercizio della soluzione stocastica poco si discosta da quella deterministica. Per testare la praticabilità della soluzione stocastica trovata, si sono imposti i valori delle variabili di controllo trovati a 2000 nuovi scenari, generati sempre con il metodo di Monte Carlo. Basandoci quindi su 2000 nuovi valori che le incertezze potrebbero assumere durante il giorno, si è verificato che la soluzione stocastica risulta praticabile nel 91% dei casi. Questo dimostra come la soluzione stocastica, a fronte di un costo di esercizio leggermente superiore garantisca una programmazione del dispacciamento molto robusta (e quindi affidabile) e adatta alla previsione del giorno prima. Ripetendo lo stesso test sulla soluzione deterministica si è invece riscontrata una praticabilità dello 0%, il che dimostra quanto la programmazione che non consideri l'influenza di incertezze sia lontano dalla pratica utilità.

Successivamente, il modello stocastico è stato usato per confrontare le soluzioni che si possono ottenere quando le incertezze vengono modellate meno accuratamente, ovvero con meno scenari. Come ci si poteva aspettare, le soluzioni trovate hanno dimostrato avere una praticabilità proporzionale alla loro accuratezza. Ciò mette in luce un limite della programmazione stocastica, ovvero che per avere soluzioni robuste necessita di modelli di incertezza con elevata accuratezza, che per contro richiedono maggior onere computazionale.

LIST OF FIGURES

LIST OF TABLES

NOMENCLATURE

Acronyms:

CCHP	Combined Cooling Heat and Power
CF-VT	Constant flow – variable temperature
CHP	Combined Heat and Power
DG	Distributed generation
DH	District heating
DHW	Domestic hot water
EF	Electric following
ETC	Evacuated-tube collector
FPC	Flat-plate collector
FR	Feasibility rate
HST	Heat storage
MC	Monte Carlo
MEMG	Multi-Energy microgrid
MG	Microgrid
MILP	Mixed-integer linear programming
MINLP	Mixed-integer nonlinear programming
OLTC	On-load tap changer
PV	Photovoltaic panel
RES	Renewable energy sources
SC	Solar collector
SOC	State of charge
SS	Stochastic solution
TF	Thermal following
TSO	Transmission system operator
VF-VT	Variable flow – variable temperature

Sets and Indices

H, h	Set/Index of buses with HST
I, i	Set/Index of buses in a MEMG

K, k	Set/Index of scenarios
M, m	Set/Index of buses with CHP
N, n	Set/Index of buses with PV
S, s	Set/Index of buses with SC
T, t	Set/index of time periods

Variables:

$E_{m,t}^{CHP}$	CHP electric energy output (kWh)
$F_{m,t}^{CHP}$	Fuel energy needed for CHP generation (kWh)
$H^{(.)}$	Thermal conduction power (kW)
$P_{i,t}, Q_{i,t}$	Active/Reactive power through the main branch from bus *i* (kW/kVar)
$P_{m/n,t}^{(.)}$	Power output of distributed generator (kW)
P_t^{def}, P_t^{sur}	Power deficiency/surplus of MEMG (kW)
$T_{i,t}^{i}$	Indoor temperature of bus *i* (°C)
$T_{i,t}^{r}$	Return temperature of bus *i* (°C)
$T_{i,t}^{s}$	Supply temperature of bus *i* (°C)
T_t^{r1}	Thermal slack bus return temperature (°C)
T_t^{s1}	Thermal slack bus supply temperature (°C)
$V_{i,t}$	Voltage of bus *i* (p.u.)
$q^{(.)}$	Thermal energy flow (kWh)
$q_{h,t}^{TS,0}$	Initial thermal energy stored in HST (kWh)
$q_{h,t}^{TS}$	Thermal energy stored in HST at timestep *t* (kWh)
$q_{h,t}^{TSC}$	Charged Thermal energy by HST at bus *h* (kWh)
$q_{h,t}^{TSD}$	Discharged Thermal energy by HST at bus *h* (kWh)
$q_{i,t}^{DHW}$	DHW demand of bus *i* (kWh)
$q_{i,t}^{SH}$	Space heating demand of bus *i* (kWh)
$q_{i,t}^{TC}$	Setting indoor temperature demand of bus *i* (kWh)
$q_{i,t}^{bill}$	Thermal energy of customer thermal usage bill (kWh)
$q_{i,t}^{laod}$	Thermal energy demand of bus *i* (kWh)
$q_{m/s,t}^{(.)}$	Thermal energy output of distributed generator (kWh)
q_t^{def}, q_t^{sur}	Thermal energy deficiency/surplus of MEMG (kWh)
q_t^{slack}	Thermal energy exchanged at the thermal slack bus (kWh)
$v_{m,t}^{fuel}$	Fuel consumption of CHP (m^3)
$\beta_{h,t}^{TSC}$	Binary decision of HST charging
$\beta_{h,t}^{TSD}$	Binary decision of HST discharging

CHAPTER 1
INTRODUCTION

According to the European Environment Agency, in 2017 greenhouse gas emissions in the European Union were distributed as shown in Fig. 1.1. As we can see the sector responsible for the highest contribution is the energy supply sector, with an overall 28% [1]. In order to tackle climate change and to foster radical decarbonizations of all States members, ambitious binding targets were set. By 2030 all EU-members agreed on cutting greenhouse gas emissions by 40% compared to 1990 levels and to cover at least 32% of final energy consumptions with renewable energy sources [2].

Integrating such a great portion of renewable energy sources (RES) will be challenging for current distribution network operators due to RES high variability and difficulty to modulate their output generation. For this reason, a whole heap of research is undergoing to enhance distribution systems' flexibility while also promoting RES penetration.

In recent years, the paradigm of energy distribution has been challenged, suggesting that traditional centralized energy production strategies may not be the most efficient for the energy scenario we are heading to. Hence, interest in distributed generation strategies has been intensifying and all energy utilities are now evolving towards decentralized systems.

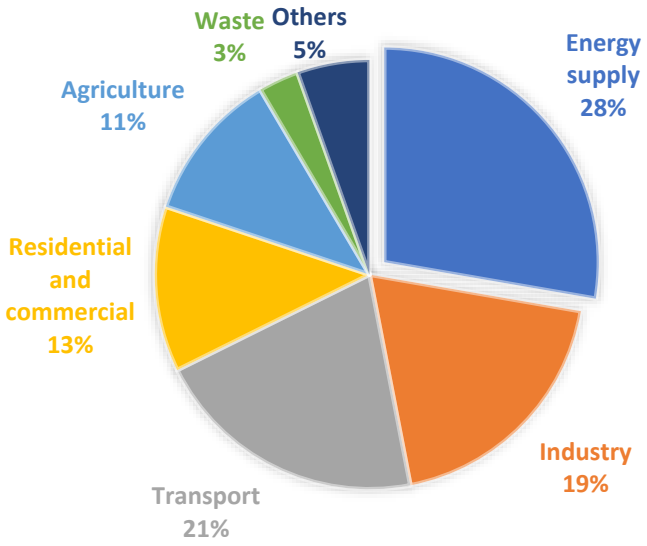

Fig. 1.1 EU greenhouse gas emissions by source sector in 2017

1.1 Distributed Energy Resources

Decentralized distribution systems are based on the concept of "local production of energy for local consumption" [3]. In this type of distribution networks, energy supply is secured by small distributed generation units (DGs) installed close to the load demand either by network utilities or private investors. Meeting load demand thanks to local energy sources results in a wide range of benefits in terms of techniques and economics. First, DGs generation alleviate load demand on the installed network node, resulting in an overall reduction of transport energy losses and transmission and distribution lines congestions. Second, they guarantee a more sensitive tracking and response to local load demand, hence providing a higher voltage stability and lower operating costs due to peak hour control [4]. Third, by enabling energy generation from different nodes of the systems, it takes full advantage of local RES output, which is not uniformly distributed on the territory. In turn, this allows utilities to reduce penalties cost for environmental care.

According to their generation controllability, DGs can be classified into two groups, i.e. dispatchable and non-dispatchable [5]. Dispatchable DGs, such as micro-turbines and fuel cells, have cost-effective operation and good reliability since their output can be controlled according to how much fuel is consumed. Non-dispatchable DGs instead, such as solar collectors (SCs) and wind turbines, are environmentally friendly sources and benefit from many economic incentives from governments. Current distribution networks rely on a combination of both DGs types to simultaneously achieve overall economic profit, system reliability and environmental benefits [6].

In the following subsections, a short introduction is given of the components considered in the MEMG model built in this thesis work .

1.1.1 Solar Photovoltaics

In 2019 the solar photovoltaic (PV) installed capacity in the European Union reached 16.7 GW, representing an astonishing 104% increase over the 8.2 GW added in 2018, which was the greatest installed capacity introduced among all other energy sources [7]. This clearly shows how much European countries are counting on this technology to reach the 2030 energy targets.

When connecting this technology to distribution networks, system operators must make sure that its active power injection will not cause excessive voltage deviations or unexpected power flow reversals. Historically, reactive power (Var) controls such as OLTC and capacitors banks used to be employed when distribution networks had a relatively small load and voltage fluctuations and significant changes in average load occur relatively slowly [8]. However, these components cannot cope with the variability of PV generation, which is strongly affected by weather conditions happening on much shorter timescales. More like, they could be operated on short timescales, but this would result in a drastic reduction of their switches lifetime [8].

A much more efficient and overall convenient method is represented by appropriately controlling the DC/AC inverter connecting PVs to the grid. Indeed, this

technology can provide much faster active power control and can also be employed to inject or consume reactive power, hence allowing them to perform voltage regulation and VAR control.

1.1.2 **Combined Heat and Power**

When power plants are integrated with heat recovery systems, Combined Heat and Power units (CHPs) are formed. Combining together the generation of both power and heat carriers results in higher overall plant efficiency. When this type of system is furtherly integrated with devices allowing cooling generation Combined Cooling Heat and Power units (CCHPs) are formed, hence allowing the simultaneous dispatch of three energy vectors.
More accurately, CHP systems are named differently according to their maximum electrical capacities, namely:

- *Cogeneration* if $P^{max} > 1\ \mathrm{MW_e}$.
- *Small scale cogeneration* if $50\ \mathrm{kW_e} \leq P^{max} < 1\ \mathrm{MW_e}$.
- *Micro-cogeneration* if $P^{max} < 50\ \mathrm{kW_e}$.

Current CHP technologies and their field of applications are shown in Fig. 1.2.

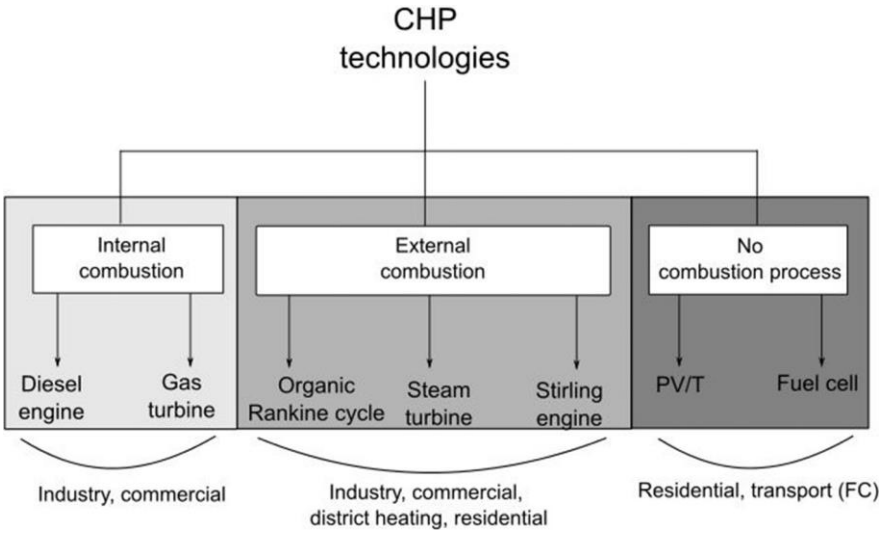

Fig. 1.2 Main CHP technologies and their fields of application [10]

Fig. 3.3Thanks to its size scalability and high primary energy usage efficiency, there is a growing interest surrounding CHPs. As evidence of this, the European Union endorsed this type of technology as a viable solution to climate change mitigation [9].

Small scale and micro-CHPs can also be installed in decentralized distribution networks, hence allowing the system operator to take full advantage of their multi-energy outputs. One of the most intriguing applications of these technologies relates to the possibility of renewable energies integration. Among the most investigated CHP system using renewable energy sources solar, biofuel and biomass are the main ones [10]. Thus, renewable energy-based micro-CHP systems can be a solution to significantly lower greenhouse gas emissions and secure energy supply. They also can facilitate energy access in rural areas, where energy infrastructures are not available and current fossil fuel-based solutions pose important environment, health, and economic issues.

1.1.3 Solar collector

Southern European countries benefit from a significant amount of irradiance throughout the year. This makes solar-driven technologies very attractive for both power and heat generation. While all devices for direct power generation are built around the photovoltaic panel, different solutions are available for direct heat generation. Three main categories can be found in the market: *Stationary compound parabolic collectors* (CPC), *Flat-plate collectors* (FPC) and *Evacuated-tube collectors* (ETC) [11]. While the first category is mostly employed for high-temperature industrial uses, the second and the third find many domestic applications such as domestic water and space heating. In Italy, solar-thermal installations are strongly supported by government incentive Conto Termico, which aims at helping the country covering 33% of final thermal energy usage with RES by 2030 to comply with EU targets [12].

FPCs are by far the most used type of collector. Usually, a transparent glass covers the absorbing plate, but many applications with no glass or multiple glasses are also available. When the sun radiation flows through the glazed cover, the absorber plate heats up, transferring its thermal energy to the operating fluids in the tubes. Then, the output heat is either consumed by customers or stored in specific tanks. For locations with a temperate climate, such as most of the Italian regions, this is the most efficient and cost-effective solution. For colder areas, ETCs are typically used instead.

1.1.4 Thermal storage

When considering thermal storage devices (HSTs) in a thermal distribution system we are increasing the flexibility of the system. Just like most commonly know electric storage units, i.e. batteries, HST allows to uncouple heat generation from the thermal load demand. Hence, this component does not only allow to redistribute heat production during the day, but it also allows higher energy usage efficiencies. As it will be explained in 3.3 when CHPs are equipped with HST its operation is not subject to bounding control strategies and its flexibility is significantly enhanced.

1.2 Multi-Energy Microgrids

Although distributed energy systems management is more challenging than traditional centralized systems, network operators can benefit from a wide range of advantages. However, these systems reveal an intrinsic limit when unexpectedly high unbalances between loads and generation occurs, requiring additional dispatchable resources (at higher cost) to equilibrate the system [13]. This could be the case of distributed systems with high RES penetration or networks with low supply redundancy. In these kinds of situations, the operating flexibility of the system can be further enhanced by coupling together systems using different energy carriers (e.g. power and heat).
By doing so, the coupled system will become even more complicated to coordinate, but it will also provide a margin for higher efficiency solutions. Let's consider, for example, an unexpected wind power peak in a winter night. In situations like this customers have a low electric and a high thermal load. Instead of requesting heat from the local CHP,

the excessive wind power can be used to run an electric boiler, hence reducing the overall operational cost.

When referring to a multi-energy microgrid (MEMG) the combination of a small electric distribution network, i.e. a microgrid (MG), together with a district heating (DH) is intended, where both electrical and thermal energies are supplied to costumers. To couple the two distinct systems, devices influencing both systems at the same time are needed, such as CHP, electric pumps or electric boilers. In the following subsections, an overview of electrical and thermal networks will be given.

1.2.1 Electrical microgrids

Microgrids (MG) are defined as small electrical distribution networks characterized by a large penetration of DGs, whose coordination is controlled by a local operator. This cluster of DGs can operate both in grid-connected or islanded mode. In the islanding mode, the MG operator's main target is to maintain the system stable while meeting customers' loads. In grid-connected operation instead, the MG operator can exchange power with the upper-level transmission system. Therefore, in this operation mode, the MG operator will try to maximize its profits by opportunely coordinating local generation and transactions with the main grid.

From the electrical systems point of view, MGs are connected to the transmission network by electrical substations, where step-down transformers adapt the transmission voltage level to the lower distribution level, typically 400V.

1.2.2 District heating systems

The distribution network of a district heating (DH) network usually consists of supply and return pipes that deliver heat, in the form of hot water or steam, from the point of generation of the heat to the end consumers [14], [15]. Fig. 1.3 shows an example of a DH with a primary, secondary and tertiary network, each of them separated by substations, supplying different types of customers.

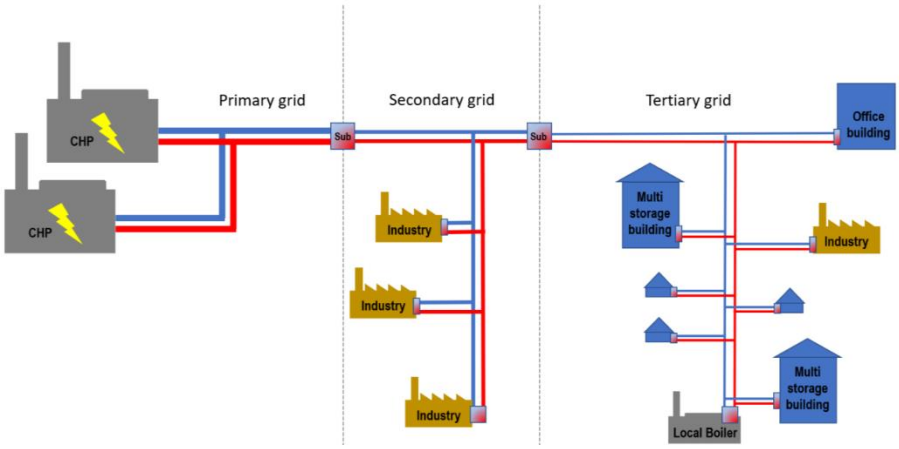

Fig. 1.3 Example of DH system feeding multiple types of consumers

Following the trend of power distribution networks, DHs are also moving towards decentralized systems using heat from multiple distributed generation facilities. This gives DH a huge potential for exploiting low-temperature sources like RES generation (such as geothermal, solar thermal, biomass) and wasted heat coming from

industries. However, integrating these types of sources poses some technical challenges which are currently undergoing. In fact, because DH networks need certain pressures to operate properly, DH are always pressurized systems; this makes the supply temperature network to take over values above 100°C, resulting in high heat losses and impossibility to include low-temperature sources. To overcome these issues, the current trend leans towards using pre-insulated pipes to lower the supply temperature – eventually until 50°C – and installing "booster units" at the consumer side[16]. This will not result only in reduced transport losses but could also allow low-temperature sources to be integrated.

Due to their high energy usage efficiency and the possibility to exploit RES, DH systems are expected to play a key role in the decarbonization of European countries.

1.3 Introduction to Optimization

Any problem involving decision making calls for planning, designing and operating in an optimal manner to reduce (or maximize) the related outcomes. Indeed, in our daily life, we come across different sorts of decisions we have to take; some of them involve complicated problems, many others refer to much simpler matter, such as finding the lowest-priced item in the store or taking the shortest path to reach a certain destination. In any of these cases, we need to ponder the variables involving the underlying problem and find the optimum solution that would allow us to reach the minimum cost, commuting time, etc. However, as the system describing the problem becomes more complicated (i.e. more variables and constraints are considered) optimal decisions become harder to take and they cannot be based only on expertise and intuition. Solving these types of problems becomes more challenging, leading to complexities related to multi-objective criteria, uncertainties of the parameters describing the system and so on.

A much better alternative was provided when the advance of computers and computational theory made it clear that by formulating tasks in a mathematical form, solving optimization problems was much more practical. Nowadays, mathematical optimization has become an essential support in all branches of engineering, economics, finance, chemistry, biology, etc. In particular, mathematical optimization is a fundamental tool for energy utilities when dealing with the planning, sizing and operating the energy system.

In conclusion, mathematical optimization can be defined as *the process of maximizing and/or minimizing one or more objectives without violating specified design constraints, by regulating a set of variable parameters that influence both the objectives and the design constraints* [17].

1.3.1 Building a model

The first step to take in the optimization process is developing an appropriate model. When referring to developing a model we mean the process of identifying and expressing in mathematical terms the objective, the variables, and all the constraints of the problem [18].

An *objective* is a quantitative measure of the performance of the system that we want to optimize. In some applications, two or more objective may be needed to satisfy different requests. For example, electrical utilities may want to minimize energy losses or the operational cost consequent to the dispatching of the system. Of course, the problem solution is going to be different whether we consider the first or the second objective. If both objectives were deemed together, the solution would result in a tradeoff between the two single objectives.

The *variables* or *unknowns* are the components of the model for which we want to find values. In an optimization problem, we can distinguish between two types of variables: decision and state variables. The first type involves those variables we are able to control and we wish to optimize; the second type, instead, regards those additional variables used to describe the system and that are determined once the decision variables are fixed. Following the previous example, possible decision and state variables involved in an optimal energy dispatch could be the power production of controllable sources (e.g. by CHP) and the volume of fuel consumed respectively.

The *constraints* are the functions that describe the dynamic of the system, the relationships among the variables and that define the allowable values for the variables. They can be stated either in an equality or inequality form. In the electrical grid, for example, the voltage on every bus is bounded within an admissible range.

A set of decision variables that fully satisfies all the constraints is called a *feasible solution* (even if it does not minimize the objective function) [17].

1.3.2 **Determining the problem type**

The second step to take in the optimization process is determining in which category of optimization the model belongs to. This step is exceptionally important since it will determine which algorithm/method and software better apply to the considered problem. Fig. 1.4 provides a helpful perspective of optimization taxonomy, mainly focusing on the subfields of deterministic problems with only one objective.

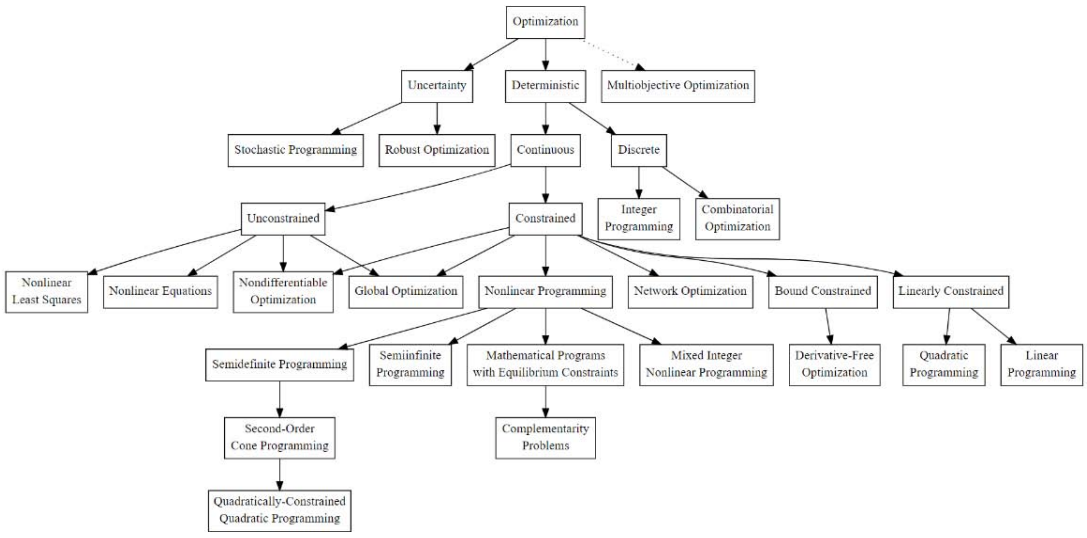

Fig. 1.4 Optimization taxonomy scheme [19]

- ***Continuous Optimization*** **vs** ***Discrete Optimization***
  In a generic model, variables may take on values from a discrete set or, in other cases, from a set allowing any real value. When a model is defined by only discrete variables - often a subset of integers - we have a *discrete optimization* problem. More specifically, when the subset of integers is bounded to binary values (0-1) we are handling a *binary optimization* problem. On the other hand, models with all continuous variables are *continuous optimization* problems. According to the considered case - a mixture of the above cases is actually the most typical case - different solving methods are available. Usually, continuous optimization problems tend to be easier to solve; the smoothness of the functions means that the objective and constraint function values at a point x can be used to deduce information about points in the surroundings of x [18]. Although, thanks to the recent enormous progress of computing technology, handling discrete optimization problems efficiently it is also possible. Lastly, it is worth mentioning that many discrete optimization problems can be reverted to a sequence of continuous subproblems, thus allowing continuous optimization algorithms to be used.

- ***Unconstrained Optimization*** vs ***Constrained Optimization***
  When the optimization variables are limited by some equality or inequality constraint, we have a *constrained optimization* problem. When they are not, we have instead an *unconstrained optimization* problem. Because most practical problems are limited by constraints, unconstrained problems usually have more theoretical than practical values [17]. Finding a solution to these types of problems is still very relevant when constrained problems are reformulated into unconstrained problems, eliminating a constraint and replacing it with a penalty factor.

  Another noteworthy aspect relates to the type of constraints used. Indeed, constrained problems can be also classified according to the nature of the constraint (e.g. linear, nonlinear, convex).

- ***Single-Objective*** vs ***Multi-Objective***
  As previously mentioned, model variables have to be optimized following a certain objective. Generally, the optimization of problems modelling physical systems involves tradeoffs among conflicting objectives. Another example relevant to energy utilities could be the optimization of energy dispatch while trying to minimize the operational cost and the CO_2 penalties coming from the usage of fossil fuel sources. Many times, problems with multiple objectives are reformulated in a single-objective form by either forming a weighted combination of the different objectives or by substituting some of the objectives with constraints [20]

- ***Deterministic Optimization*** vs ***Nondeterministic Optimization***
  In *deterministic optimization*, the data used to describe the system is assumed to be known accurately. This assumption is not just very unrealistic - leading to solutions that do not describe closely real-life systems - but it is also very inadequate because the mathematical solution found may be physically unfeasible – in the energy dispatch, this may lead to excessive fuel bought or problematic power flow solutions. If input data uncertainty and variability are incorporated into the model, we will have a *non-deterministic optimization* problem. There are different methods to handle this type of problem, namely divided into stochastic and heuristic methods. In the following subsection, this category will be further discussed.

1.3.3 **Optimization under uncertainty**

As previously mentioned, when modelling real physical systems, input data is never perfectly known. This is due to a variety of reasons, the main two being measurement and forecasting errors.

When including measured data in our model, we must accept that the *real value* of the measured entity does not exist; this is because every measurement is affected by some intrinsic variability. Apart from the measured entity itself, many other sources of errors may be involved in the measurement process; some of them are attributable to the measuring tool, the measuring method or even the operator in charge of the process. In electrical engineering, a good example of the aforementioned issues is represented by the resistance evaluation of resistors [21].

Similarly, when dealing with forecasting data, we must rely on predictions coming from algorithms using historical data and statistical theory. As much as the forecasting methods might be sophisticated, it is impossible to fully capture the randomness and aleatory nature of some parameters. Thus, because there is no way to perfectly predict data, the robustness of deterministic models' solutions is very limited. For example, in current distribution networks, electricity utilities need to model the uncertainty of PV generation so that the power-flow solutions will be appropriate.

For the above-mentioned reasons, to properly model our problem, we must be able to properly model uncertainties. In the past, empirical safety factors were used to compensate the propagation effects of uncertainties. As Messac observed though, this often *resulted in overly conservative designs, increasing the probability businesses may lose their competitive edge in terms of cost and performance* [17]. Later on, mathematical frameworks were developed, achieving algorithms that can guarantee insensitiveness to data uncertainty to a significant extent.

1.3.4 Uncertainties in MEMG

Different types of uncertainty affect the MEMG optimal operation. All of them can be grouped among three categories [3]:

- *Energy uncertainties*
  MEMGs with high RES penetration are severely affected by supply generation uncertainty, due to RES variability. Also, because MEMG generation consists of multiple small size DGs, when load unexpected variations occur, balancing the system is more challenging than in centralized systems; thus, load demand uncertainty is also very relevant to MEMG.

- *Economic uncertainties*
  The dispatch of MEMGs operating in grid-connected mode is significantly affected by the energy price upon which transactions with the upper-level transmission grids are made. Thus, it is also important to find optimal solutions under different price realizations.

- *Technical uncertainties*
  Some parameters defining devices' performances, such as efficiencies, cannot be perfectly estimated. This uncertainty makes the architecture of the MEMG model uncertain as well.

In the literature, energy uncertainties are the most investigated sources of uncertainty and, for this reason, this thesis work will consider only this type of uncertainty.

1.4 Thesis Contribution

The contributions given by this thesis work are listed as follow:

- Investigating MEMGs operation control strategies under uncertainties. In this work, three uncertainty sources were considered: electric load, outdoor temperature, and solar irradiation.
- A fully constrained MEMG formulation is formulated, considering multiple devices and both electrical and thermal network constraints.
- An optimal one-stage stochastic optimization method is proposed to handle multiple uncertainties.
- Analyzing how solar collector devices influence the MEMG dispatch under uncertain sun irradiation.

1.5 Thesis Structure

The description of each chapter included in this thesis is as follows:

- *Chapter 1* gives an introduction of the components considered in the considered MEMG and a short background of optimization theory.

- *Chapter 2* and *Chapter 3* describe the models of the electrical and thermal distribution systems. Both network and components constraints are presented.
- *Chapter 4* presents the stochastic optimization formulation. Both deterministic and stochastic solution methods are outlined. Then the Monte Carlo sampling method and Simultaneous backward reduction technique are introduced.
- *Chapter 5* describes the test system used to perform the numerical simulations. A description of how uncertainties were modeled is also given.
- *Chapter 6* illustrates and discusses the results obtained from the numerical simulations of both deterministic and stochastic problems. To compare these two solutions a feasibility check was carried out, also including some other simulation cases.
- *Chapter 7* presents the conclusions, the main findings, and recommendations for future works.

CHAPTER 2
ELECTRICAL DISTRIBUTION SYSTEM MODELLING

In this chapter, the constraints used to model the microgrid dynamics are going to be presented. As previously mentioned, by referring to the term *microgrid* we are considering all the components influencing the power flow of the multi-energy system. In order to obtain a correct representation of the system, an accurate set of equations, also called formulation, needs to be used.

The MG model is composed of the following elements:

- Distribution network
- Photovoltaic solar panels (PV)
- Combined Heat and Power units (CHP)
- Loads

2.1 Distribution Network

The model of the distribution network needs to satisfy several constraints that must describe correctly the power-flow. Different models of power-flow problems are used in the literature. For this thesis work, a linearized version of the DistFlow will be used.

2.1.1 Power Flow Model

To solve the power-flow problem the *DistFlow* formulation used by references [22] and [23] was applied. Let's consider a unidirectional single branch radial distribution circuit like the one in Fig. 2.1, having *n-1* branches and *n* buses. It is

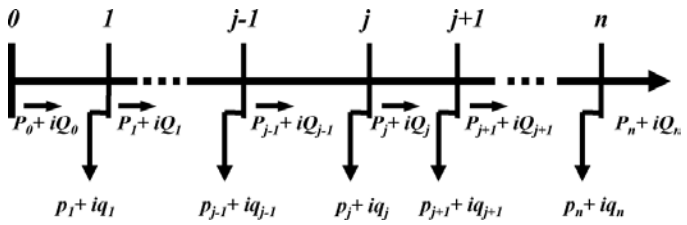

Fig. 2.1. One-line schematic diagram of a radial system [22]

worthwhile mentioning that by considering a circuit with unidirectional flows we are referring to current distribution networks, where reverse flows are considered consequences of faults.

In the figure, the 0-bus, also called *slack-bus,* is connected to the upper-level grid at the reference constant voltage V_0. Lines are modeled by a series impedance $z_l = r_l + jx_l$ and loads are considered as constant power sinks, with apparent power equal to $S_L = P_L + jQ_L$.

If the power supplied from the upper grid, $S_0 = P_0 + jQ_0$, is known then the apparent power and the voltage at the receiving end of the branch can be evaluated as follows:

$$S_1 = S_0 - S_{loss} - S_{L1} = S_0 - z_l I^2 - S_{L1} = S_0 - z_l \frac{|S_0|^2}{V_0^2} - S_{L1}$$

$$V_1 = V_0 - z_1 I_0 = V_0 - \frac{S_0^*}{V_0}$$

Applying the same procedure to all the other branches, we obtain the following general equations:

$$P_{i+1} = P_i - r_i \frac{P_i^2 + Q_i^2}{V_i^2} - P_{L1} = P_i - r_i \frac{P_i^2 + Q_i^2}{V_i^2} - p_{i+1}^c + p_{i+1}^g \quad \forall i \qquad 2.1$$

$$Q_{i+1} = Q_i - x_i \frac{P_i^2 + Q_i^2}{V_i^2} - Q_{L1} = Q_i - x_i \frac{P_i^2 + Q_i^2}{V_i^2} - q_{i+1}^c + q_{i+1}^g \quad \forall i \qquad 2.2$$

$$V_{i+1}^2 = V_i^2 - 2(r_i P_i + x_i Q_i) + (r_i^2 + x_i^2) \frac{P_i^2 + Q_i^2}{V_i^2} \quad \forall i \qquad 2.3$$

where,

V_i: voltage at bus *i*;
P_i, Q_i: real and reactive power flowing on branch *i +1*;
p_i^c, p_i^g : active power consumed and generated by bus *i*;
q_i^c, q_i^g: reactive power consumed and generated by bus *i*;

2.1.2 **Linearization of DistFlow**

To alleviate the computational burden of the model, a simplified formulation of the distribution network can be applied using the following assumptions:

- The nonlinear terms of the DistFlow model can be neglected.
  Using a linearized formulation of the power-flow problem is largely accepted in the literature [24]. Turitsyn *et al.* [8] demonstrated that the solution obtained using this approximation is almost indistinguishable from the model based on Eqq. 2.1-2.3. This is because the nonlinear terms $\propto (P_i^2 + Q_i^2)/V_i^2$, which

represent the branch losses, are much smaller (o^4) than the linear terms P_i, Q_i, representing the active and reactive power flowing through the branches.

- The square of the difference between the voltage on the *j*-bus and the reference voltage on the slack bus is neglectable. This approximation is accepted as long as the deviation of voltages across the distribution network is kept within an allowed range. This leads to expression $V_i^2 \approx V_0^2 + 2V_0(V_i - V_0)$.

Under these two approximations, the formulation of the distribution network becomes:

$$P_{i+1} = P_i - p_{i+1}^c + p_{i+1}^g \quad \forall i \tag{2.4}$$

$$Q_{i+1} = Q_i - q_{i+1}^c + q_{i+1}^g \quad \forall i \tag{2.5}$$

$$V_{i+1} = V_i - \frac{r_i P_i + x_i Q_i}{V_0} \quad \forall i \tag{2.6}$$

Once we defined the set of equations used to solve the Power Flow problem, we have to find an efficient technique that can be used to implement the set of constraints. In the literature, most of the solution techniques apply either graph properties or the incidence matrix to automate the implementation process. Alternatively, as it was done in this thesis, simulation can be run coding each set of constraints.

For radial distribution networks simulations, we used a code based on a topology matrix containing all the topological information about the considered distribution network. By following this procedure, the *DistFlow* formulation can be studied on any kind of radial circuit, no matter the number of nodes nor the number of lateral branches.

A simple example is used to illustrate this approach. Fig. 2.2. shows a radial circuit with five buses and four branches.

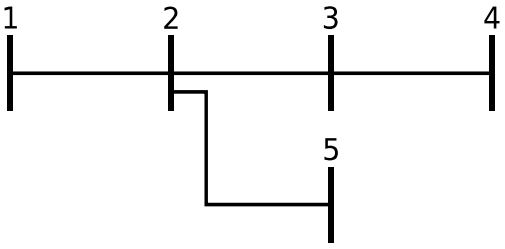

Fig. 2.2 A simple radial distribution network

The topology of this circuit is entirely described in Table 2.1, whose columns represent:

1st column	Name of the branch
2nd column	Starting bus of the branch
3rd column	Ending bus of the branch, also called *to bus*
4th column	The resistance of the branch
5th column	The reactance of the branch

6th column	1 if the branch is the first parallel branch 2 if the branch is the second parallel branch 0 if the branch has no parallel branches
7th column	Active power withdrawn by *to bus*
8th column	Reactive power withdrawn by *to bus*
9th column	1 if the branch is an end-branch 0 if the branch is not an end-branch
10th column	Source branch

Table 2.1 Topology matrix for a simple radial circuit

1st	2nd	3rd	4th	5th	6th	7th	8th	9th	10th
1	1	2	r	x	0	P	Q	0	0
2	2	3	r	x	1	P	Q	0	1
3	3	4	r	x	0	P	Q	1	2
4	2	5	r	x	2	P	Q	1	1

The DistFlow program then writes all the constraints in a block matrix format in order to solve the following linear system:

$$A_{n\_branch,n\_branch} \cdot x_{3 \cdot n\_branch,1} = b_{3 \cdot n\_branch,1}$$

The block matrix ***A*** shown in Table 2.2 contains on the first, second and third block-line the constraints related respectively to active power, reactive power, and voltage. It is worth to notice that while *P* and *Q* are entities related to branches, *V* are instead related to buses.

Table 2.2 Block matrix containing all the power-flow constraints

$$A = \left[\begin{array}{cccc:cccc:cccc} 1 & -1 & 0 & -1 & 0 & 0 & 0 & 0 & 0 & 0 & 0 & 0 \\ 0 & 1 & -1 & 0 & 0 & 0 & 0 & 0 & 0 & 0 & 0 & 0 \\ 0 & 0 & 1 & 0 & 0 & 0 & 0 & 0 & 0 & 0 & 0 & 0 \\ 0 & 0 & 0 & 0 & 0 & 0 & 0 & 0 & 0 & 0 & 0 & 0 \\ \hdashline 0 & 0 & 0 & 0 & 1 & -1 & 0 & -1 & 0 & 0 & 0 & 0 \\ 0 & 0 & 0 & 0 & 0 & 1 & -1 & 0 & 0 & 0 & 0 & 0 \\ 0 & 0 & 0 & 0 & 0 & 0 & 1 & 0 & 0 & 0 & 0 & 0 \\ 0 & 0 & 0 & 0 & 0 & 0 & 0 & 1 & 0 & 0 & 0 & 0 \\ \hdashline 0.02 & 0 & 0 & 0 & 0.04 & 0 & 0 & 0 & 1 & 0 & 0 & 0 \\ 0 & 0.02 & 0 & 0 & 0 & 0.04 & 0 & 0 & -1 & 1 & 0 & 0 \\ 0 & 0 & 0.01 & 0 & 0 & 0 & 0.04 & 0 & 0 & -1 & 1 & 0 \\ 0 & 0 & 0 & 0.02 & 0 & 0 & 0 & 0.08 & -1 & 0 & 0 & 1 \end{array}\right] \begin{matrix} \\ \\ \\ 1^{st} \\ \\ \\ \\ 2^{nd} \\ \\ \\ \\ 3^{rd} \end{matrix}$$

In Table 2.3 instead, the unknown vector ***x*** and the known term ***b*** are displayed. It should be noticed that ***b*** contains the active and reactive load of every bus and the reference voltage, in per-units, at the slack-bus.

Table 2.3 Vectors x and b

$$x = \begin{bmatrix} P_1 \\ P_2 \\ P_3 \\ P_4 \\ \hdashline Q_1 \\ Q_2 \\ Q_3 \\ Q_4 \\ \hdashline V_1 \\ V_2 \\ V_3 \\ V_4 \end{bmatrix} \qquad b = \begin{bmatrix} 0.2 \\ 0.8 \\ 0.4 \\ 0.2 \\ \hdashline 0.1 \\ 0.3 \\ 0.1 \\ 0.1 \\ \hdashline 1 \\ 0 \\ 0 \\ 0 \end{bmatrix}$$

2.1.3 **Voltage deviation**

As already mentioned before, to ensure a good power-quality on the system, the magnitude of voltages deviation across the circuit must be kept within acceptable bounds:

$$V^{\min} \le V_i \le V^{\max} \qquad \forall i,t$$

Considering a per-units base, the voltage constraint can be written as:

$$1-\varepsilon \le V_i \le 1+\varepsilon \qquad \forall i,t \tag{2.7}$$

For transmission systems, the voltage deviation ε is typically set to $\varepsilon = \pm 5\%$ while for distribution system $\varepsilon = \pm 10\%$ is mostly accepted.

2.1.4 **Slack bus**

Considering a grid-connected case, the behavior of the power slack bus needs to be modeled in order to guarantee a correct power exchange between the MG and the main grid.

When the power production in the MG is not enough to fulfill the customers' loads, the MEMG operator must buy electricity from the main grid, P^{def}. On the contrary, when power production of the DG exceeds the customers' needs, electricity must be injected into the main grid, P^{sur}.

The power effectively exchanged between the MG and the main grid in every time step, which is a result of the optimization problem, is modeled by Eq. 2.8:

$$P_t^{slack} = P_t^{def} - P_t^{sur} \qquad \forall t \tag{2.8}$$

Where P^{slack} is defined in Eq. 2.9 following the notation of the variables used in the simplified DistFlow formulation:

$$P_t^{slack} = P_{l,t} \qquad \forall i,t \tag{2.9}$$

2.1.5 **Branch capacity**

All transmission lines must operate under their maximum power capacity, which can be expressed by an apparent power limit. This limit depends not just on the material properties but also on the length of the lines. While excessive power flowing in short lines will result in overheating damages to the lines and to the system equipment, the maximum capacity for long lines must also consider stability concerns.
As it will later be explained, loads maintain constant power factor throughout the day, hence keeping the active and reactive power flowing in each branch proportional to each other. Following reference [24], the capacity limit of each branch is represented by the active power constraint in Eq. 2.10 to avoid quadratic constraints inclusion:

$$-P^{cap} \le P_{i,t} \le P^{cap} \qquad \forall i,t \tag{2.10}$$

2.2 **Photovoltaics Solar Panel**

The installation of PVs in a distribution network results in an active power injection into the system. Thereby, power demand on each bus is reduced as well as the active power flow in the connecting branch, decreasing significantly transmission losses.

Different from fossil fuel power sources, PVs production cannot be planned. Even though its output can be predicted by modelling the movements of the sun, it still relies strongly on atmospheric conditions. The two major parameters influencing the efficiency of these systems are the irradiance and temperature of the cell, which depend on the clearance of the sky and wind speed, respectively.

2.2.1 **Output power production**

In the literature, many PV dynamics models have been proposed to properly describe output power production. Basaran *et al.* [25] used a model based on the equivalent electric circuit of PV cells, achieving simulation results very close to reality. In another work [26], the hourly energy production is obtained by multiplying the hourly ideal output generation by a derating factor which takes into account several parameters reducing the performances of the PV panel.

For the purpose of this study, a more general model is considered. The output power produced throughout the day by the PV system can then be evaluated as follows:

$$\begin{aligned} p_{n,t}^{PV} &= P^{PV,\max} \cdot PV_t^{index} \qquad \forall n,t \\ &= P^{PV,\max} \cdot G_t^{index} \qquad \forall n,t \end{aligned} \tag{2.11}$$

where $P^{PV,\max}$ is the PV installed capacity and PV_t^{index} is the daily power output profile multiplier. This profile is assumed to have the same outline of the

irradiance in a reference day and is therefore achieved by scaling the irradiance profile by its maximum value.

2.3 Combined Heat and Power units

As already introduced in Chapter 1, Combined Heat and Power (CHP) units differ not just on the size but also on the different types of technology they rely on. Several types of models can, therefore, be found in the literature according to the type of unit considered and modelling accuracy required.

In this section, some of the most used formulations to model the electrical and thermal behavior of CHP will be presented, while also motivating the choice of the model used in this thesis.

2.3.1 Output power and heat recovery

For large size units, namely defined as Cogeneration units, works like [27]-[28] make use of the *polyhedrons method* in order to describe the CHP feasible operating region. Following this approach, the power and heat dispatched by the unit can be described by a convex combination of the corner points defining the operating region:

$$p = \sum_{k=1}^{M} \alpha^k x^k$$

$$q = \sum_{k=1}^{M} \alpha^k y^k$$

Where x^k and y^k are the power and heat production for the k^{th} corner point and α^k are positive weights whose summation must be equal to the binary variable representing the operating status of the unit.

It is worthwhile mentioning that this procedure can also be extended to CHP with a non-convex feasible area by dividing the region into different sub-areas.

For smaller units, micro-CHP and small scale CHP, a more general model can be implemented. Zhengmao *et al.* [29] referred his work to a Capstone's micro-turbine considering a nonlinear relation between power output and electrical efficiency:

$$\eta_{MT} = 2.767 \cdot 10^{-7} (P_{MT})^3 - 7.337 \cdot 10^{-5} (P_{MT})^2 + 6.385 \cdot 10^{-3} (P_{MT}) + 0.107$$

By using this type of formulation, all entities depending on η_{MT} would be nonlinear therefore creating a mixed-integer nonlinear programming problem (MINLP). To alleviate the computational burden, it is common practice to linearize this kind of relations using piecewise-linear functions, transforming the problem in a MILP one. Once this is done, the output heat recovered is evaluated by:

$$Q_{MTH} = \eta_H COP_H P_{MT} (1 - \eta_{MT} - \eta_L) / \eta_{MT}$$

Where η_H and COP_H represents the heat recovery ratio and coefficient of performance of the heat recovery unit. Lastly, η_L is the heat loss ratio.

Another different formulation comes from reference [24], where the heat recovered by the CHP is modeled following an energetic approach. This is the formulation considered in this thesis.

The electrical energy produced by the CHP unit is defined as:

$$E_{m,t}^{CHP} = P_{m,t}^{CHP}\tau, \quad \forall m,t \tag{2.12}$$

where $P_{m,t}^{CHP}$ is the output active power and τ is the intraday operation stage set as one hour.

The fuel energy needed to obtain that electrical energy is equal to:

$$F_{m,t}^{CHP} = E_{m,t}^{CHP} / \eta^{PGU}, \quad \forall m,t \tag{2.13}$$

where η^{PGU} is the constant electrical efficiency.

The heat recovered can finally be evaluated as:

$$q_{m,t}^{HR} = \eta^{HR}(F_{m,t}^{CHP} - E_{m,t}^{CHP}), \quad \forall m,t \tag{2.14}$$

where η_{HR} is the heat recovery factor.

2.3.2 **Outputs range constraints**

Like any other realistic dispatchable unit, CHP output power cannot exceed its nominal capacity. At the same time, the output power must also be higher than a certain threshold. Similar considerations also apply for the output heat, which must be bounded within an upper and lower bound.

Therefore, the following range constraints must be considered:

$$P^{CHP\min} \le P_{m,t}^{CHP} \le P^{CHP\max}, \quad \forall m,t \tag{2.15}$$

$$q^{HR\min} \le q_{m,t}^{HR} \le q^{HR\max}, \quad \forall m,t \tag{2.16}$$

2.3.3 **Ramping constraints**

When planning the dispatch of power units, ramping constraints must also be taken into account. Ramp rates, indeed, define how quickly power plants can change their output power and are, consequently, defined in units of power (e.g. kW) over time (e.g. one minute).

Because the grid has to maintain a constant balance between generation and demand and because ramp rates assume very different values according to the different types of power plants, choosing accurately the mix of generating units plays a key role when sizing and planning the power system. This becomes even more severe when considering grids with high penetration of RES, which can ramp up and ramp down very quickly, unbalancing the system.

The ramping constraint can then be defined as:

$$-r_{down}^{CHP} \cdot P_m^{CHP\max} \le P_{m,t}^{CHP} - P_{m,t-1}^{CHP} \le r_{up}^{CHP} \cdot P_m^{CHP\max}, \quad \forall m,t \tag{2.17}$$

2.4 **Electric loads**

In this study, loads are considered fixed, with no possibility to react to the MEMG operator's needs. As already explained in section 2.1, active and reactive power are withdrawn at each bus. The apparent power requested by the load is then:

$$S_{i,t}^{L} = P_{i,t}^{L} + jQ_{i,t}^{L}, \quad \forall i,t$$

The power demand requested by every load throughout the day can be evaluated as follows:

$$S_{i,t}^{L} = S^{L} \cdot load_{t}^{index}, \quad \forall i,t \tag{2.18}$$

where S^L is the reference bus apparent power and $load_t^{index}$ is the daily load demand profile multiplier. Once the profile with absolute values is selected, the percentage profile is obtained by scaling the load profile by its maximum value.
It should be noticed that by using Eq. 2.18 we are assuming that the power factor on every bus will stay constant during the day. This assumption is quite realistic considering that rephasing devices are widespread in current distribution networks.

CHAPTER 3
DISTRICT HEATING MODELLING

Once the electrical model of the MEMG is completed, we can now focus on the formulation of the *district heating* dynamics. By doing so, we are aiming at describing the thermal grid through which heat is produced, distributed and delivered to thermal loads.

Similar to the microgrid model, also the DH is composed of the distribution network, sources and loads. In addition to these elements, the system considered in this research is also equipped with storage units that allow a more flexible operation.

In the next sections the models of the following elements are going to be presented:

- Distribution network
- Solar collector
- Thermal storage
- Thermal loads

It is worth to notice that CHP units are key components also for the DH network since their outputs influence both electrical and thermal systems. Hence, their model could have been included either in the MG or the DH formulation. For the sake of clarity, it was reported in the previous chapter.

3.1 District Heating Network

In this study, the district heating network is modelled following a constant-flow and variable-temperature (CF-VT) strategy. Even though the fully nonlinear variable-flow and variable temperature (VF-VT) strategy can achieve better optimization results, solving this type of model in a satisfactory manner it is still rather challenging [27]. Hence, to simplify the complexity of the model, the CF-VT strategy was chosen, without losing generality.

In order to simulate correctly the dynamics of the thermal vector through the system in steady-state conditions, a *Hydraulic* and a *Thermal* model were built. The combination of these two models defines the *Heat power model*, whose structure is shown in Fig. 3.1.

From the figure, we can see that once the Hydraulic model is run, the flow ratios in all pipelines are obtained and consequently the Thermal model can be used to determine the supply and return temperatures of every bus.

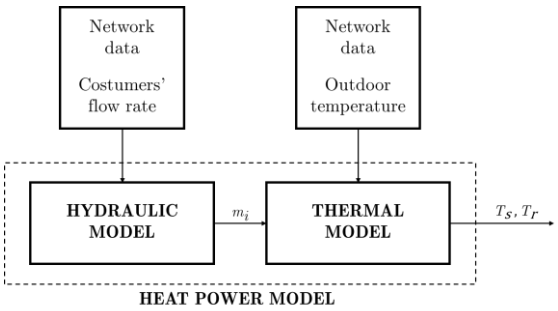

Fig. 3.1 Block diagram of the Heat power model

3.1.1 **Hydraulic flow**

Solving the hydraulic flow in a DH is very similar to solving the power flow in an electrical circuit. As shown in Table 3.1 there is a clear analogy between hydraulic and electrical laws. This consideration allows us to build the Hydraulic model following a similar procedure.

Table 3.1 Analogies between electrical and hydraulic network

Power flow	Kirchhoff's current law	Kirchhoff's voltage law	Ohm's law
Hydraulic flow	Mass conservation law	Loop pressure balance	Head loss

It is worthwhile mentioning that while in the VF-VT strategy the hydraulic network is modeled considering both flow and pressure constraints [15], in CF-VT applications, pressure constraints can be neglected [27]. This can be motivated by the fact that water pumps' consumption is largely determined by the hydraulic regimes in the network. In these situations, mass flow rates of water pumps and heat-substation are considered as decision variables so that their related costs can be optimized. On the other hand, when considering constant hydraulic regimes, the cost related to the pumps' power consumption are fixed and cannot be optimized.

For the above-mentioned reasons, this model does not consider pressure constraints in the Hydraulic model formulation. Thus, only flow rate constraints are taken into account.

According to the Mass conservation law, also known as Continuity law, when considering an incompressible fluid, the mass flowing into one node must be equal to the sum of the mass leaving the node. By applying this law on every DH bus, we can state that: the sum of all water flow rates entering a bus must be equal to the flow rates leaving the bus plus the flow consumption at each node. For both the supply and return network, this constraint is expressed by Eq. 3.1:

$$\left(\Sigma \dot{m}\right)_{in} - \left(\Sigma \dot{m}\right)_{out} = m_q \qquad 3.1$$

Where $\dot{m}$ is the mass flow running through each pipe and m_q is the mass flow either withdrawn from the supply network buses or injected into the return network buses.

Because the flow direction in both the supply and return networks is fixed, the costumer's requested flow will always leave the bus in the supply network and will always enter the bus in the return network.

As mentioned before, solving the hydraulic flow is very similar to solving the power flow problem. Therefore, when implementing this set of constraints in a code with a general pipeline system, we can take advantage of the same procedure used in section 2.1.1.

This will result in a linear system of the following form:

$$A_{n\_branch,n\_branch} \cdot x_{n\_branch,1} = b_{n\_branch,1}$$

As an example, let's consider the same simple network used when the power flow algorithm was introduced, which is here reported in Fig. 3.2:

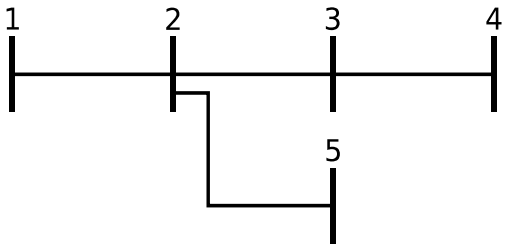

Fig. 3.2 A simple radial district heating network

In Table 3.2 the ***A*** matrix containing all the mass conservation constraints is reported. As can be observed, inside this matrix all the +1 values refer to flows entering a bus, while all the -1 values refer instead to all those flows leaving the bus.

Table 3.2 Hydraulic *A* matrix

$$A = \begin{bmatrix} 1 & -1 & 0 & -1 \\ 0 & 1 & -1 & 0 \\ 0 & 0 & 1 & 0 \\ 0 & 0 & 0 & 1 \end{bmatrix}$$

Finally, in Table 3.3 the ***x*** and ***b*** vectors are shown. While the unknown ***x*** vector contains all the flow rates variables, the know-term vector ***b*** contains all the withdrawn or injected costumers' flows.

Table 3.3 Vectors x and b

$$x = \begin{bmatrix} m_1 \\ m_2 \\ m_3 \\ m_4 \end{bmatrix} \quad b = \begin{bmatrix} 0.2 \\ 0.3 \\ 0.1 \\ 0.4 \end{bmatrix}$$

3.1.2 **Thermal flow**

Because under CF-VT strategy the hydraulic regimes of the network are invariant, the constraints that build up the Hydraulic and Thermal models are decoupled. Therefore, once the Hydraulic model is solved – and all the mass flows within each pipeline are known - the Temperature model is run, allowing the solver to calculate the supply and return temperatures at every bus of the DH.

The outlet temperature of every pipeline of both supply and return network is calculated using the *Temperature drop equation* [15]:

$$T_{out,i} = \left(T_{in,i} - T_a\right) e^{-\frac{\lambda_i L_i}{c_w \dot{m}_i}} + T_a \qquad 3.2$$

Where,

- $T_{out,i}$ outlet temperature of pipeline i;
- $T_{in,i}$ inlet temperature of pipeline i;
- T_a outdoor temperature;
- λ_i overall heat transfer coefficient for pipeline i;
- L_i length of pipeline i;
- c_w specific heat of water;
- $\dot{m}_i$ mass flow in pipeline i;

As it can be observed by Eq. 3.2, the temperature drop is defined by means of an exponential factor which makes the outlet temperature of a pipeline proportional to the mass flowing through.

Defining $T'_{out,i} = T_{out,i} - T_a$, $T'_{in,i} = T_{in} - T_a$ and finally $\Psi_i = e^{-\frac{\lambda_i L_i}{c_w \dot{m}_i}}$, we can rewrite Eq. 3.2 in the following form:

$$T'_{out,i} = T'_{in,i} \Psi_i \qquad 3.3$$

Thanks to Eq. 3.3 we can now evaluate the outlet temperature of every pipeline of the network. However, when considering a pipeline network, we need to take into account that there could be several pipelines either entering or leaving each bus. When these situations happen, the resulting temperature at the bus is a mixed temperature, which is determined by the thermal energy of every mass flow entering the bus. As the first principle of thermodynamics states, the energy of an isolated system is constant, hence the sum of the energies of the outlet flows must be equal to the sum of the energies of the inlet flows.

$$\sum_{b \in P_i^-} \left(\dot{m}_b c_w \cdot T_{in,b}\right) = \sum_{b \in P_i^+} \left(\dot{m}_b c_w\right) \cdot T_{out,i}$$

Where $b \in P_i^-$ is the set of branches entering the i-bus and $b \in P_i^+$ is the set of branches leaving the i-bus.

Since in every branch of the pipeline network flows the same fluid, the mixing temperature constraints for the supply and return network are:

$$\sum_{b\in P_i^-}\left(\dot{m}_b^s\cdot T_{in,b}^s\right)=\sum_{b\in P_i^+}\left(\dot{m}_b^s\right)\cdot T_{out,b}^s$$

$$\sum_{b\in P_i^-}\left(\dot{m}_b^r\cdot T_{in,b}^r\right)=\sum_{b\in P_i^+}\left(\dot{m}_b^r\right)\cdot T_{out,b}^r$$

In the previous constraints, the costumers' mass flows are not taken into account. When considering them, the mixing temperature constraints become:

$$\sum_{b\in P_i^-}\left(\dot{m}_b^s\cdot T_{in,b}^s\right)=\left[\sum_{b\in P_i^+}\left(\dot{m}_b^s\right)+\dot{m}_{q,i}\right]\cdot T_{out,b}^s \qquad 3.4$$

$$\left[\sum_{b\in P_i^-}\left(\dot{m}_b^r\right)+\dot{m}_{q,i}\right]\cdot T_{in,b}^r=\sum_{b\in P_i^+}\left(\dot{m}_b^r\right)\cdot T_{out,b}^r \qquad 3.5$$

As it can be noticed, the customer' mass flows withdrawn from the supply network are considered as the flows of fictitious pipelines leaving the corresponding bus. For the return network instead, the customers' injected mass flows are considered as fictitious pipelines entering the corresponding bus. This way of looking at the customer model comes from the realistic assumption that the temperature drop between each household and its heat-exchange substation is neglectable. Thus, the inlet and outlet temperature of customer mass flow coincide with those of the connected bus.

Once the equality constraints are defined, some additional inequality constraints should also be considered to ensure a satisfactory "heat quality" at every bus of the DH. Bounding the bus temperature between a satisfactory limit is very similar to the dual concept of keeping voltages in the power grid within an allowed range. Thus, all temperatures on the supply and return buses must be constrained to:

$$T^{s,\min}\le T_{i,t}^s\le T^{s,\max} \qquad 3.6$$

$$T^{r,\min}\le T_{i,t}^r\le T^{r,\max} \qquad 3.7$$

Because of the current industry tendency to include low-temperature sources to the DH, in present DH the upper bound of the supply temperature must be kept below 100°C. Therefore, common values used Eq. Eq. 3.6 are:

$$80°C\le T_{i,t}^s\le 95°C$$

For the return supply network instead, the lower bound of Eq. 3.7 is determined by health concerns. Indeed, to prevent legionella [1] contamination, the water flowing

[1] Pathogenic group of bacteria which can cause health problems

through the pipelines must always be kept above 50°C [30]. The upper and lower bounds used in this model are:

$$50°C \leq T_{i,t}^{r} \leq 65°C$$

However, for one category of buses, Eq. 3.7 assumes different values. In this DH formulation indeed, all buses with thermal generation units are allowed to feedback to the DH part of their heat. For these buses, the return temperatures are constrained by:

$$50°C \leq T_{i,t}^{r} \leq 110°C$$

The reason why the upper bound of the return temperature is so large is due to the fact that we want to take advantage of the excessive heat produced by the thermal units. By feeding back to DH part of the heat we can lower the return temperature of the slack-bus. Therefore, the heat imported from the upper-level transmission system will decrease and so will its associated exchange cost.

Let's now consider our reference simplified DH system, whose supply and return network are shown in Fig. 3.3. The solutions of the Hydraulic model for both cases have equal absolute values, but opposite signs.

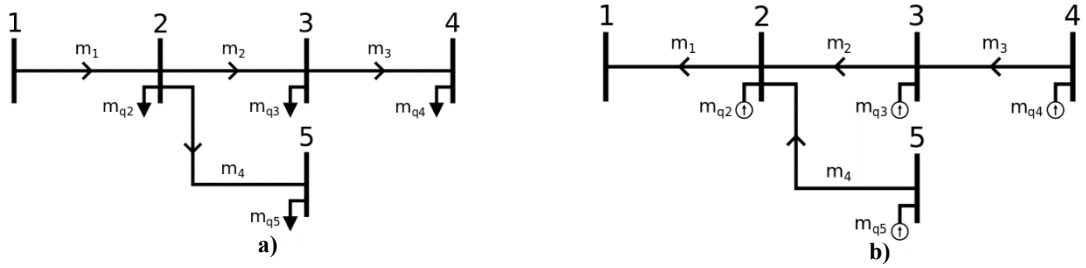

Fig. 3.3 Example of flows distribution in a simplified a) supply and b) return network

When implementing Eq. 3.4 and 3.5 inside the code, a matrix formulation was used, like in sections 2.1.1 and 3.1.1.

All the constraints for the supply network are written in the following form:

$$-\dot{m}_i \Psi_i \cdot T_i^s + \dot{m}_{down,i} \cdot T_{i+1}^s = 0$$

Where $\dot{m}_{down,i} = \sum_{b \in P_i^+} (\dot{m}_b^s) + \dot{m}_{q,i}$ is the sum of all flows leaving the bus, including customers' ones. Then, the return network constraints are expressed by:

$$\dot{m}_{up,i} \cdot T_i^s - \sum_{b \in P_i^-} \left(\dot{m}_b \Psi_b \cdot T_{b+1}^s \right) = 0$$

Where $\dot{m}_{up,i} = \sum_{b \in P_i^+} (\dot{m}_b^r) - m_{q,i}$ is the sum of all flows leaving the bus minus the customers' ones.

The Temperature model is then built up combining all the constraints of both supply and return network in only one linear system defined using a block-matrix:

$$A_{1+2 \cdot n\_branch,2+2 \cdot n\_branch} \cdot x_{2+2 \cdot n\_branch,1} = b_{1+2 \cdot n\_branch,1}$$

For this example, let's consider T_{r1} = 100°C and $\dot{m}_{q,i}$ = 0.4 kg/s.

The ***A*** matrix, shown in Table 3.4, is composed of the 1st block containing all the constraints related to supply temperatures and the 2nd block containing all those related to return temperatures. Because of the logic the code follows to build the A matrix, one additional constraint had to be written at the bottom.

Table 3.4 A matrix of the Temperature model

$$A = \left[\begin{array}{cccccccccc}
0.8 & 0 & 0 & 0 & 0 & 0 & 0 & 0 & -0.78 & 0 \\
-0.38 & 0.40 & 0 & 0 & 0 & 0 & 0 & 0 & 0 & 0 \\
0 & -0.18 & 0.2 & 0 & 0 & 0 & 0 & 0 & 0 & 0 \\
-0.18 & 0 & 0 & 0.20 & 0 & 0 & 0 & 0 & 0 & 0 \\
\hdashline
0 & 0 & 0 & 0 & 0.60 & -0.38 & 0 & -0.18 & 0 & 0 \\
0 & 0 & 0 & 0 & 0 & 0.20 & -0.18 & 0 & 0 & 0 \\
0 & 0 & 0 & 0 & 0 & 0 & 0 & 0 & 0 & 0 \\
0 & 0 & 0 & 0 & 0 & 0 & 0 & 0 & 0 & 0 \\
\hdashline
0 & 0 & 0 & 0 & -0.98 & 0 & 0 & 0 & 0 & 1.00
\end{array}\right] \begin{array}{l} 1^{st} \\ \\ \\ \\ \\ \\ 2^{nd} \\ \\ \\ \end{array}$$

Table 3.5 shows the ***x*** and ***b*** vectors. While the unknown ***x*** vector contains all the temperature variables, the know-term vector ***b*** contains all zeros.

Table 3.5 Vector *x* and *b* of the Temperature model

$$x = \begin{bmatrix} T_{s2} \\ T_{s3} \\ T_{s4} \\ T_{s5} \\ \hdashline T_{r2} \\ T_{r3} \\ T_{r4} \\ T_{r5} \\ \hdashline T_{s1} \\ T_{r1} \end{bmatrix} \quad b = \begin{bmatrix} 0 \\ 0 \\ 0 \\ 0 \\ 0 \\ 0 \\ 0 \\ 0 \\ 0 \\ 0 \end{bmatrix}$$

3.1.3 **Slack bus**

Similarly to the model of the power grid slack-bus in section 2.1.3, also the slack-bus of the DH is connected to an upper-level transmission system. The heat exchanger thermally linking the two systems is schematically shown in Fig. 3.4.

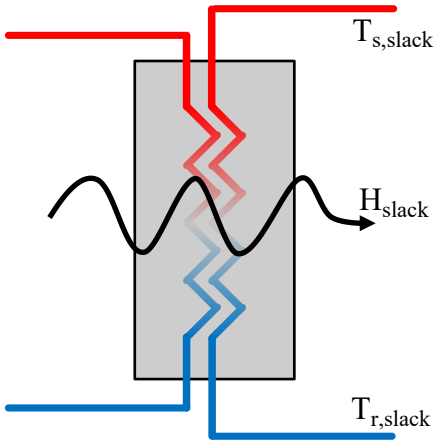

Fig. 3.4 Heat exchanger between transmission system and DH

When the sum of heat demand from the loads together with the discharged heat of the HST is greater than the heat produced by the thermal units, the DH will have to buy heat from the transmission system. On the contrary, when the sum of the heat demand together with the charged heat from the HST is lower than the heat production within the DH, all the excessive heat can be feedback to the transmission system. Thus, when in case of deficiency, the DH will have to import q^{def}, while in case of surplus the DH will feedback q^{sur} .

In order to consider this binary behavior of the slack bus, the following constraint is needed:

$$q_t^{slack} = q_t^{def} - q_t^{sur} \tag{3.8}$$

The heat exchanged with the transmission system, q^{slack}, can also be express by means of the temperatures on its buses:

$$q_{i,t}^{slack} = m_{l,t} c_w (T_{i,t}^{s,slack} - T_{i,t}^{r,slack}) \tag{3.9}$$

3.2 **Solar Collectors**

Among heating generation units considered in this system, apart from the CHP, also solar thermal collectors are included. Exactly like PV panels, the output production of these units is proportional to the irradiance of the sun and thus, their output production follows its same profile throughout the day.

To simulate realistically the performances of solar collectors, the model employed in [31] was used as a reference. The parameters of the glazed FPC considered are listed in Table 3.6.

Table 3.6 Parameters of reference solar collector

Glazed flat-plate collector		
Area	A	2.3 m^2
Zero loss efficiency	η_0	0.79
Heat loss coefficients	a_1	4.04 W/(m^2K)
	a_2	0.0182 W/(m^2K)

3.2.1 **Efficiency**

The efficiency of solar collectors in steady-state operation is expressed by the following non-linear equation [11]:

$$\eta = \eta_0 - a_1 \frac{(T^m - T^a)}{G} - a_2 G \left(\frac{T^m - T^a}{G} \right)^2$$

Where

η_0 Zero loss coefficient
T^m Average fluid temperature
T^a Outdoor temperature
a_1 Linear heat loss coefficient
a_2 Quadratic heat loss coefficient
G Irradiance

As can be observed the conversion from irradiance to thermal energy is severely influenced by both outdoor temperature and fluid temperature. A more compact expression of the previous equation can be obtained using the reduced temperature difference T_m^*:

$$\eta = \eta_0 - a_1 T_m^* - a_2 G \left(T_m^* \right)^2 \qquad 3.10$$

Thus, when considering n_p number of installed collectors, each of them having an aperture area A, the output heat production throughout a day is equal to:

$$q^{sol} = n_p (\eta \cdot G \cdot A) \qquad 3.11$$

3.2.2 **Output heat production**

Although using Eq. 3.11 in our formulation will allow us to achieve very accurate results, it will also transform our model in a non-linear problem, increasing remarkably the computational burden. In order to maintain a MILP formulation while trying to consider also the influence of temperature, the following method was used.

Firstly, constant temperatures of the water flowing through the collector were assumed according to the considered season. Then, using the same reference irradiance profile G^{index} employed in section 2.2.1 and a reference outdoor temperature profile, the heat

output of the indicated solar collector, $q^{sol,}$ is evaluated. In this way, the values obtained will be influenced by both hourly changing parameters G and T^a.

Similarly to what was done in section 2.2.1, q^{sol} is scaled by the maximum value during the day, $q^{sol,\max}$. This allows us to boil q^{sol} down to a percentage profile. Finally, the approximated heat production throughout the day is evaluated as:

$$q_{s,t}^{sol} = q^{sol,\max} \cdot G^{index} \quad \forall s,t \tag{3.12}$$

3.3 Thermal Storage

Other key role components inside the model are represented by thermal storage units (HSTs), which in this work are provided to all buses with thermal units (CHP and SC). The presence of HST is particularly important for the dispatch of CHP units to decouple the electrical and heat systems - or, in other words, microgrid and district heating – connected by the CHP units.

If thermal storage units were not considered, then the dispatch of CHP should follow either an *electrical-following* (EF) or a *thermal-following* (TF) strategy. In the first case, the CHP units would be dispatched in order to match electrical loads, while in the second case, CHP would be requested to "follow" the thermal loads. The consequences of operating under these strategies force the system operator to deal with several issues.

Typically, in grid-connected microgrids, CHPs operate under the TF strategy since the power imbalance can be compensated by exchanging power with the transmission grid. Operating the system in the following way was shown to have a severe problem when trying to exploit RES generation [15][26][31]. During wintertime, for example, heat demand could be very high while at the same time electric demand is very low. In these situations, because CHP outputs are coupled to one another, both heat and power dispatched will be very high. This will cause an oversupply of electricity in the grid and leading to important RES curtailment, wind in particular.
In islanded operation, instead, microgrids are usually operated under EF [29]. This is quite reasonable since, from the system operator point of view, a power imbalance can generally have more dangerous outcomes than a thermal mismatch. However, the burden of this strategy is born by costumers, whose thermal comfort might be compromised.
In both cases, the control of the MEMG becomes rigid, not allowing the MEMG operator to take full advantage of the flexibility that CHP could offer.

On the other hand, if thermal storage units are considered, all the excessive heat produced by the CHP can be stored and released when heat demand is high. Thus, the two outputs of the CHP become uncoupled, giving the MEMG operator a lot more flexibility when planning the system dispatch.

In addition, providing thermal storage also to solar collectors can further enhance the flexibility of the system. All buses provided with such components will play an active role when optimizing the heat exchanged with the DH.

3.3.1 **Charging and discharging**

The first behavior that must be modeled to make the HST operate properly is that in each timestep the status of the unit should never be charging or discharging at the same time. In order to capture this binary dynamic, the following constraint must be satisfied:

$$\beta_{h,t}^{TSC} + \beta_{h,t}^{TSD} \leq 1 \quad \forall h,t \tag{3.13}$$

Where β_{TSC} and β_{TSD} are the two binary variables for charging and discharging respectively. As Eq. 3.13 shows, during each timestep the HST can either charge or discharge but can also stay neutral, thus making the left-hand side equal to zero.

In every timestep the heat stored or released by the HST must be bounded between some realistic bounds:

$$0 \leq q^{TSC} \leq \beta_{h,t}^{TSC} \cdot q_h^{TSC,\max} \quad \forall h,t \tag{3.14}$$

$$0 \leq q^{TSD} \leq \beta_{h,t}^{TSD} \cdot q_h^{TSD,\max} \quad \forall h,t \tag{3.15}$$

where $q^{TSC,max}$ and $q^{TSD,max}$ are the maximum allowed heat charged and discharged withing each timestep, typically set equal to 1/8 of the total heat capacity of the HST.

3.3.2 **Heat storage status**

Another constraint that must be satisfied by the HST is that the available thermal energy of each unit at the initial and final hour of the day must be the same.

$$q_{h,0}^{TS} = q_{h,24}^{TS} \quad \forall h,t \tag{3.16}$$

Another useful way to write the same constraint is by using the State Of Charge (SOC) parameter, which is defined as:

$$SOC(\mathrm{t}) = \frac{q_{h,t}^{TS}}{q_h^{TS,\max}} 100 \quad \forall h,t$$

Thus, leading to:

$$SOC(0) = SOC(24)$$

It is worth noticing that without this constraint the solver might decide to only charge or discharge the unit throughout the day. This could definitely be a realistic behavior of the HST, but it might take away part of the relevant decision-making role it was intended to be given to this component.

Like any other physical component, the heat stored inside the HST must be bounded within a range:

$$0 \leq q_{h,t}^{TS} \leq q_h^{TS,\max} \quad \forall h,t \tag{3.17}$$

3.3.3 **Stored heat energy during the day**

Finally, the heat available at the end of every timestep must be updated considering the following constraint:

$$q_{h,t}^{TS} = \eta^{TS} q_{h,t-1}^{TS} + \eta^{TSC} q_{h,t}^{TSC} - \frac{q_{h,t}^{TSD}}{\eta^{TSD}} \quad \forall h,t \tag{3.18}$$

Where, η_{TS} is used to model the self-discharging losses, while η_{TSC} and η_{TSD} are the charging and discharging efficiency rates.

3.4 **Household Thermal Loads**

On every bus of the DH, except the slack-bus, a cluster of households are supposed to be connected. Every cluster is composed of *nb* number of buildings each of them having *nf* number of floors. When estimating the building's thermal load, adequate results can be obtained by calculating heat losses and gains based on a steady-state heat transfer analysis [33]. More accurate representations can be achieved by considering the discrete building thermal inertia, which, in real-world scenarios, affects significantly the indoor temperature dynamics during every timestep. For the sake of simplicity, in this work, we considered a steady-state regime.

3.4.1 **Domestic Hot Water**

An important part of the total heat load requested by a household is due to the domestic hot water (DHW). This component includes the heat needed for all usages (dishwashing, clothes washing, cleaning, and personal hygiene) with the exception of space heating. In 2012 in Canada it was estimated that about 20% of the yearly residential energy consumption was due to DHW [34], which was more than all the electrical energy consumption.

In order to evaluate the total DHW needed by a household during a day, the procedure proposed in [11] was used following these assumptions:

- The average volume of water consumed during a day for DHW application (L_w) can be assumed equal to 50 liters per person
- The requested hot water temperature (T_{wh}) must be equal to 45°C
- The inlet cold water temperature (T_{wc}) is set equal 15°C
- The number of people living in every floor of every building (N_p) is equal to 4

The daily value of heat demand of DHW requested at every bus by the *nb*-buildings can then be evaluated as:

$$Q^{DHW,daily} = nb \cdot nf \cdot \left[L_w \cdot N_p \cdot \rho \cdot c_w \frac{(T_{wh} - T_{wc})}{3600} \right] \tag{3.19}$$

where, ρ = 1000 m^3/kg is the water density and c_w= 4.186 kJ/(kg·K) is the specific heat of water. Eq. 3.19 is divided by 3600 to define the output heat in kWh.

Once the total heat needed during a day was calculated, the DHW profile of a residential building found in [35] was used to calculate the hourly heat demand. The reference DHW profile is shown in Fig. 3.5.

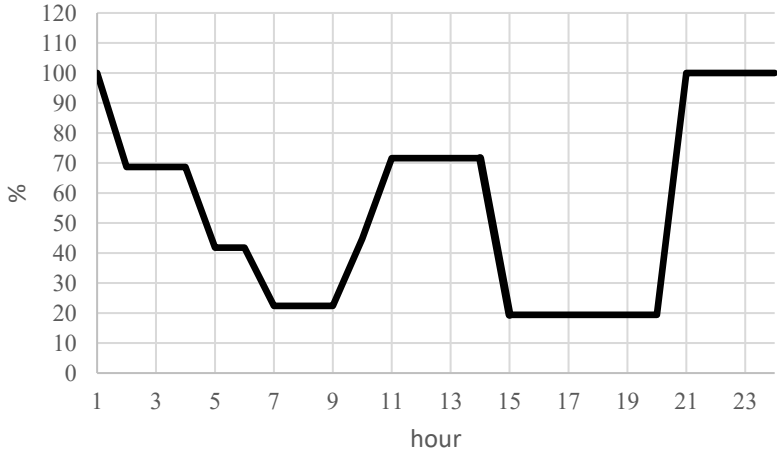

Fig. 3.5 Daily DHW profile of a residential building

To determine the amount of heat corresponding to each hour of the day, the area under the given profile was evaluated summing all the trapezoids defined under each timestep. Then, every hourly trapezoid was divided by the total area in order to define the percentage heat corresponding to each hour, creating the DHW^{index}.

Finally, the absolute value of DHW requested throughout the day was calculated by:

$$q_{i,t}^{DHW} = Q^{DHW,daily} \cdot DHW_t^{index} \qquad \forall i,t \tag{3.20}$$

3.4.2 **Space heating**

When trying to maintain a setpoint indoor temperature inside the building, additional heat must be withdrawn from the DH. Specifically, the total thermal power supplied from the air conditioning consists of two components: the heat needed to compensate the thermal transfer through the building envelope and the heat needed to reach the setpoint indoor temperature. The space heating demand can be then evaluated as:

$$H_{i,t}^{SH} = H_{i,t}^{BE} + H_{i,t}^{Ti}, \quad \forall i,t \tag{3.21}$$

In an electrical analogy, the thermal transfer rate flowing through the building envelope can be evaluated as follow:

$$H_{i,t}^{BE} = \frac{T_{i,t}^{in} - \tilde{T}_t^{am}}{R^T}, \quad \forall i,t \tag{3.22}$$

Eq. 3.22 states that the thermal power flowing from the indoor space to the ambient environment can be evaluated by temperature difference over the building's shell divided by the thermal resistance of the building envelope.

Because the setpoint indoor temperature may vary across the day, the air conditioning systems must be able to compensate the indoor thermal power variations. Hence, the following contribute must be considered:

$$H_{i,t}^{Ti} = c^{air}\left(\frac{dT^{in}}{dt}\right), \quad \forall i,t \tag{3.23}$$

As it can be observed from Eq. 3.22 and Eq. 3.23, the space heating term depends on the household physical properties and the air conditioning systems setpoint indoor temperature. Because of the large buildings' thermal inertia, the indoor temperature variations are negligible within each intra-day operation interval. Thus, the indoor temperature can be considered constant in each timestep. Consequently, Eq. 3.21 can be rewritten using a discrete state model, where the temperatures and space heating terms are modeled in hourly states, as:

$$H_{i,t}^{SH} = c^{air}\frac{\left(T_{i,t}^{in} - T_{i,t-1}^{in}\right)}{\tau} + \frac{T_{i,t}^{in} - \tilde{T}_{t}^{am}}{R^{T}}, \quad \forall i,t \tag{3.24}$$

Eq. 3.24 can finally be expressed in terms of kWh by multiplying all terms by the timestep length τ.

$$q_{i,t}^{SH} = c^{air}\left(T_{i,t}^{in} - T_{i,t-1}^{in}\right) + \frac{T_{i,t}^{in} - \tilde{T}_{t}^{am}}{R^{T}}\tau, \quad \forall i,t \tag{3.25}$$

In order to provide some flexibility to the thermal loads' definition, the indoor temperature can be set within a comfortable range:

$$T^{in,\min} \le T_{i,t}^{in} \le T^{in,\max}, \quad \forall i,t \tag{3.26}$$

3.4.3 **Thermal load**

Finally, the complete thermal load requested from every bus of the DH is given by summing the DHW and the space heating demand:

$$q_{i,t}^{HL} = nb\left(q_{i,t}^{DHW} + q_{i,t}^{SH}\right), \quad \forall i,t \tag{3.27}$$

Because the daily DHW demand remains constant throughout the year, the thermal load is influenced only by the indoor and outdoor temperatures. It is worth to mention that some other external parameters influence the indoor temperature dynamic, like the solar radiation incident on the surface of the building and the heat given off by occupants' metabolism or other domestic appliances. If a more detailed house thermal model was needed, reference [36] could be considered.

3.5 Thermal Energy Bill

Following [24] approach, *the customers' thermal load bill payment is based on minimal heat energy required to keep the comfortable indoor temperature. The limits of the comfortable indoor temperature are applied to calculate this thermal energy as the follows,*

$$q_{i,t}^{HL,bill} = \begin{cases} \left(T_{i.t}^{in,\min} - \tilde{T}_t^a\right)\tau / R^T & if\ \tilde{T}_t^a < T_{i.t}^{in,\min} \\ 0 & if\ \tilde{T}_t^a \geq T_{i.t}^{in,\min} \end{cases}, \quad \forall i,t \tag{3.28}$$

As a result, this minimal thermal energy usage is influenced only by the varying ambient temperature rather than the setpoint indoor temperature. Consequently, the thermal usage bills do not depend on the indoor temperature control and the customers' economic benefits are secured.

3.6 Withdrawn Thermal energy

Lastly, constraint 3.29 defines the heat requested by every bus from the DH, which is determined by the heat load and, for buses with heat generators, also by the heat produced and heat exchanged with the HST.

$$q_{i,t}^{DH} = q_{i,t}^{HL} + q_{m,t}^{CHP} + q_{s,t}^{SC} + \left(q_{h,t}^{TSC} - q_{h,t}^{TSD}\right), \quad \forall i,m,s,h,t \tag{3.29}$$

CHAPTER 4
OPTIMIZATION

4.1 **Stochastic Optimization**

When uncertain parameters follow a probability distribution that is known or can be estimated, stochastic optimization can be applied. This method takes advantage of the data probability information to model the uncertain parameters as random variables to which the theory of probability can be used [37]. Typically, because continuous probability distributions are more complex to model, most problems prefer using discrete distributions.

The purpose of stochastic optimization is to find a feasible solution for all the possible values that the uncertain parameters may take, while also minimizing (or maximizing) the objective function. Stochastic problems can be interpreted as problems where the decision-maker must initially make an optimal decision when the value of some data is still unknown (e.g. PV generation) by exploiting the known probability distribution; once the uncertainty on the parameters is realized, the decision-maker must minimize the consequences of his former decision by taking a recourse action.

Each possible realization of the uncertain parameter, also called a *scenario*, can be obtained using either previous historical data or by randomized sampling techniques (this topic will be further discussed in the next section). Now that the *scenario* concept was introduced, the purpose of stochastic optimization can be reformulated as finding a solution that is feasible for all the possible scenarios while also minimizing (or maximizing) the total cost, given by the sum related to the first and second decision.

Stochastic optimization programming can be generally expressed in mathematical terms using a *two-stage stochastic linear optimization* form. A brief overlook of this formulation will now be presented, following reference [38].

Let $x \in \mathbb{R}^n$ and $y \in \mathbb{R}^m$ be two variables and let the set of scenario be given by $\Omega = \{\omega_1, \dots, \omega_K\} \subseteq \mathbb{R}^r$, where r is the number of scenarios representing the uncertain parameters. The stochastic problem is stated as:

$$\begin{aligned} \min_x \quad & z = c^T x + \mathbb{E}\Big[Q\big(x, \omega\big)\Big] \\ s.t. \quad & Ax = b \\ & x \geq 0 \end{aligned} \tag{4.1}$$

where

$$\begin{aligned} Q\left(x,\omega\right) &= \min_{y}\ q^{T}y(\omega) \\ s.t. \quad & T(\omega)x + W(\omega)y = h(\omega) \\ & y \geq 0 \end{aligned} \qquad 4.2$$

Eq. 4.1 and Eq. 4.2 define the first-stage and the second-stage problem, respectively. In the first-stage, x is the decision variable, c^T represents the cost coefficients of the objective function and $\mathbb{E}[Q(x,\omega)]$ denotes the expected value of the optimal solution of the second-stage problem. This last term can be seen as the expected recourse cost. Then, this first linear problem minimizes the first-stage direct cost while satisfying the first-stage constraints, $Ax = b$.

In the second-stage instead, y becomes the decision variable and q^T denotes the cost coefficient. The second-stage objective function is subject to some recourse function, $Tx + Wy = h$, whose parameters are all dependent on the scenario realization. Then, this second linear problem minimizes the cost of the recourse action needed once the scenarios' value is realized.

Thus, to summarize, the first-stage decision must be taken before the uncertain parameters are realized so that the solution is feasible for all possible scenarios. Once the first-stage optimal solution is fixed, the variabilities on parameters are cleared, and the realization of scenarios becomes available. Putting together the information of the first-stage decision and the scenarios' realization, in the second-stage, a recourse action is taken, and a second optimal solution is determined.

A noteworthy piece of information is that the first-stage decision variable x does not depend on which type of scenario is realized in the second-stage. This very important property is defined as *non-anticipativity* and it is employed to model the fact that when deciding upon an uncertain future, we cannot take advantage of the knowledge we will gain in the future [39].

One of the most common techniques to solve a two-stage stochastic linear problem is by formulating as a *deterministic equivalent* problem.

Let us assume that the uncertain parameter has a finite number of possible realization (i.e. scenarios), denoted as $\omega_1, \ldots, \omega_K$ with respective probabilities $\rho_1, \ldots, \rho_K$, so that $\sum_k \rho_k = 1$. Then, the expectation term in Eq. 4.1 can be written as:

$$\mathbb{E}[\,Q(x,\omega)] \triangleq \sum_{k=1}^{K} \rho_k Q(x,\omega_k) \qquad 4.3$$

The original two-stage stochastic linear programming model can be expressed as a linear system in the following way:

$$
\begin{aligned}
\min_{x,y_1,\ldots,y_K} \quad & c^T x + \rho_1 q^T y_1 + \rho_2 q^T y_2 + \ldots + \rho_K q^T y_K \\
s.t. \quad & Ax = b \\
& T_1 x + W_1 y_1 = h_1 \\
& T_2 x + W_2 y_2 = h_2 \\
& \vdots \qquad\qquad \ddots \qquad\qquad \vdots \\
& T_K x + W_K y_K = h_K \\
& x \geq 0, \; x \in \mathbb{R}^n \\
& y_k \geq 0, \; y_k \in \mathbb{R}^m
\end{aligned}
$$

Note that for stochastic linear programs the deterministic equivalent notation is just another linear system. In a more compact form this can be written as:

$$
\begin{aligned}
\min_{x,y_1,\ldots,y_K} \quad & c^T x + \sum_{k=1}^{K} \rho_k q^T y_k \\
s.t. \quad & Ax = b \\
& T_i x + W_i y_i = h_i \\
& x \geq 0, \; x \in \mathbb{R}^n \\
& y_k \geq 0, \; y_k \in \mathbb{R}^m
\end{aligned}
\qquad 4.4
$$

As we can observe, the first-stage decision variable, x, does not depend on any second-stage parameter, hence satisfying the *non-anticipativity* property. Also, because we solve for all the first and second-stage decisions simultaneously, x must be feasible for every scenario and its value represents (in some sense) as an overall optimum solution [39].

One of the major drawbacks of stochastic optimization problem is that it requires a large number of scenarios to properly model the nature of the uncertainty [40]. Thus, the better we want to approximate the uncertainty and more scenarios are needed. Stochastic programming, hence, can provide robust solutions but is penalized by high computational cost. Another weakness of the stochastic optimization is due to the fact that it can only guarantee constraint satisfaction by accurately knowing probability distribution data, which is not always easy to obtain.

4.1.1 **Robust optimization**

A more recent approach to handle uncertainty in optimization problems is represented by *robust optimization*. Different from classical stochastic programming, robust optimization is characterized by the following features [41]:

- uncertainty randomness is captured by using uncertainty sets instead of probability distributions. An uncertainty set contains all the values an uncertain parameter can take on.
- while stochastic optimization relies on optimal *expected* values, robust optimization searches for an optimal solution within the *worst case*. By doing so, the solution found is immune against any uncertainty realization.

Unfortunately, exploring the applications of this technique is not in the interest of this thesis. For a more comprehensive picture of robust optimization theory, reference [42] can be consulted.

4.2 Solution Method

The optimal operation model proposed in this thesis work aims to maximize the total operating profit of the MEMG over 24 hours by optimizing the day-ahead decision variables, i.e. the CHP electric power output $P_{m,t}^{CHP}$ and the thermal storage operation state $\beta_{h,t}^{TSC/D}$ and $q_{h,t}^{TSC/D}$.

In a MEMG such as the one described, multiple uncertainties affect the system operation. In this thesis we are going to consider three sources of uncertainty:

- ***Electric load demand:***
  Utilities rely on a lot of historical data to forecast electricity demand. As much as more and more variables influencing customers' behavior are considered, the predictions made can never be completely accurate. While in traditional distribution networks, the operator can count on a large reserve capacity to fix any mismatch in the power flow solution, the MEMG operator has only a limited number of dispatchable units. Thus, because transactions with the main grid should try to be reduced, capturing this type of uncertainty is very relevant for a MG.

- ***Outdoor temperature:***
  Similar to the electric load demand, also outdoor temperature predictions can never be perfect. The uncertainty on this parameter affects the space heating demand component and propagates up to the total thermal load demand definition. Therefore, this uncertainty affects the thermal flow in the DH, hence making the management of thermal storage units more challenging.

- ***Sun irradiance:***
  Differently from the previous uncertainties, irradiance in a sky-clear day can be precisely estimated using the equations of the movement of the Sun. Unfortunately, the sky is not always clear, since the weather conditions vary considerably during the day. Thus, both PVs and SCs output generation will be uncertain, hence affecting both power and thermal flow problems.

To capture the nature of these three uncertainties, the deterministic optimization problem is reversed into a stochastic optimization problem. To highlight the differences between these two approaches, simulations will be run using both deterministic and stochastic problems.

In Table 4.1 all variables used in the model are listed showing whether they are decision or state variables while also differentiating continuous from discrete/binary variables. As we can see, the decision variables of our model are the CHPs output power

and all variables concerning the HSTs dynamic. To properly model the binary status of HSTs, our model also includes two binary variables, i.e. $\beta_{TSC/D}$.

Table 4.1 Variables used in the model

Variable name	*Type of variable*	*Nature of variable*
P	*State*	*Continuous*
Q	*State*	*Continuous*
V	*State*	*Continuous*
P^{CHP}	*Decision*	*Continuous*
E^{CHP}	*State*	*Continuous*
F^{CHP}	*State*	*Continuous*
v^{fuel}	*State*	*Continuous*
P^{def}	*State*	*Continuous*
P^{sur}	*State*	*Continuous*
T^{s1}	*State*	*Continuous*
T^{s}	*State*	*Continuous*
T^{r1}	*State*	*Continuous*
T^{r}	*State*	*Continuous*
T^{i}	*State*	*Continuous*
q^{slack}	*State*	*Continuous*
q^{def}	*State*	*Continuous*
q^{sur}	*State*	*Continuous*
q^{CHP}	*State*	*Continuous*
q^{TSC}	*Decision*	*Continuous*
q^{TSD}	*Decision*	*Continuous*
β_{TSC}	*Decision*	*Binary*
β_{TSD}	*Decision*	*Binary*
$q^{TS,0}$	*Decision*	*Continuous*
q^{TS}	*State*	*Continuous*
q^{laod}	*State*	*Continuous*
q^{DHW}	*State*	*Continuous*
q^{SH}	*State*	*Continuous*
q^{TC}	*State*	*Continuous*
q^{bill}	*State*	*Continuous*

4.2.1 **Deterministic optimization**

The deterministic optimization problem considers deterministic input data, which can be easily obtained from a wide range of open-source databases. In our case, the deterministic input data matches the mean values of the probability distribution curves upon which scenarios will be generated.

The objective function that our problem must optimize is represented as follows:

$$\min C_{CHP} + C_{OM} + C_{ex}^{el} + C_{ex}^{th} - C_{rev}^{el} - C_{rev}^{th} \qquad 4.5$$

The first element defines the cost of the fuel consumed by the CHP units:

$$C_{CHP} = \sum_{t \in T} \sum_{m \in M} C^{fuel} V_{m,t}^{fuel} \tag{4.6}$$

The second element represents the operation and maintenance cost of CHPs, PVs, and SCs respectively:

$$\begin{aligned} C_{OM} &= \sum_{t \in T} \left(\sum_{m \in M} C^{CHP} P_{m,t}^{CHP} \tau + \sum_{n \in N} C^{PV} P_{n,t}^{PV} \tau + \sum_{s \in S} C^{SC} q_{s,t}^{SC} \right) \\ &= C_{OM}^{CHP} + C_{OM}^{PV} + C_{OM}^{SC} \end{aligned} \tag{4.7}$$

The third and fourth terms identify the exchange cost with their upper-level transmission systems, as shown in Eq. 4.8 and Eq. 4.9, respectively:

$$C_{ex}^{el} = \sum_{t \in T} C^{buy,el} P_t^{def} \tau - C^{sell,el} P_t^{sur} \tau \tag{4.8}$$

$$C_{ex}^{el} = \sum_{t \in T} C^{buy,el} P_t^{def} \tau - C^{sell,el} P_t^{sur} \tau \tag{4.9}$$

In conclusion, the last two terms describe the revenues of the MEMG operator coming from the electrical and thermal energy sold to the customers:

$$C_{rev}^{el} = \sum_{t \in T} \sum_{i \in I} Pr^{el} P_{i,t}^{EL} \tau \tag{4.10}$$

$$C_{rev}^{th} = \sum_{t \in T} \sum_{i \in I} Pr^{th} q_{i,t}^{bill} \tag{4.11}$$

4.2.2 **Stochastic optimization**

Differently from the deterministic problem, we now want to optimize the decision variables to guarantee feasible operation under uncertainties. In this thesis work, uncertainties are modeled as scenarios generated by the Monte Carlo sampling technique, which will be explained in the next section. Hence, in the stochastic optimization problem, the solver will look for a solution that must be feasible for all *K* scenarios (initially in our case, *K* = 200). For this reason, the solution to our problem must have only one set of decision variables and *K* sets of state variables. From the coding point of view, this can be achieved following these steps:

1) Define *K*-sets of each state variable. Let's y be a generic state variable; then
$$y = \{y_1, \dots, y_K\}$$
2) Every constraint depending on state variables or uncertainties must be rewritten *K* times. Every *k*-constraint will then be defined by the corresponding *k*-state variable and *k*-scenario value. If decision variables are included, the same variables must be used for every *k*-constraint. Let's consider the general constraint C
$$C: \ x + y = a$$

Where x is a decision variable, y is a state variable and a is an uncertain parameter. Then, the C constraint will generate *K* constraints each of them having the following form:

$$c_k \in C : x + y_k = a_k \ \forall k$$

3) Any cost term of the deterministic objective function related to either state variables or uncertain parameters must be isolated. Let's consider the following generic deterministic objective function:

$$\Theta_{DET} = f_1(x) + f_2(y, \omega)$$

Where f_1 is a cost function depending only on a decision variable, x, and f_2 a cost function depending on either a state variable, y, or a scenario, ω.
All cost terms in the form of f_2 must be summed together and multiplied by ρ_k, which is the probability of the *k*-scenario to happen. The stochastic objective function will then be defined as:

$$\Theta_{STO} = f_1(x) + \sum_{k=1}^{K} \rho_k \cdot f_{2,k}(y_k, \omega_k)$$

Which will be subject to the set of constraints $C = \{c_1, \dots, c_k\}$.

As can be observed from the above-mentioned solution method, the solver must look for an optimal solution that satisfies all *K* constraints at the same time. By doing so, the solution found is not going to be the best solution for any single scenario, but it is going to be the best solution *overall*.

The deterministic objective function given by Eq. 4.5 will then assume the following stochastic form:

$$\min C_{CHP} + C_{OM}^{CHP} + \sum_{k=1}^{K} \rho_k \left[C_{OM,k}^{PV} + C_{OM,k}^{SC} + C_{ex,k}^{el} + C_{ex,k}^{th} - C_{rev,k}^{el} - C_{rev,k}^{th} \right] \qquad 4.12$$

Eq. 4.12 shows that the only two terms depending on decision variables are the cost terms related to the CHP active power $P_{m,t}^{CHP}$. All the other terms depend either on state variables or scenarios. More precisely,

$C_{OM,k}^{PV}$ and $C_{OM,k}^{SC}$	Depend on the sun irradiation uncertainty
$C_{ex,k}^{el}$ and $C_{rev,k}^{el}$	Depend on the active power flowing on the first branch, which comes from the solution of the power flow problem
$C_{ex,k}^{th}$ and $C_{rev,k}^{th}$	Depend on the supply and return temperatures of the thermal slack bus, which are determined once the thermal flow is solved

One last thing that should be noticed is that in this solution approach we cannot take a recourse action, thus making our problem a single-stage problem even though we are using a two-stage programming formulation.

4.3 Scenario Generation

When historical data regarding uncertainties realization is not available to perform stochastic optimization simulations, sampling methods must be used. Sampling techniques can be divided into two categories: probability and non-probability sampling. Probability sampling techniques are based on randomization; hence every sampled element gets an equal chance to be selected among a set of other sampled elements. Among these techniques, Monte Carlo sampling methods are some of the most widely used.

4.3.1 Monte Carlo Sampling

Monte Carlo (MC) sampling method is a computational technique to randomly sample a probability distribution; reference [43] points out three main reasons to use MC methods:

- Estimate density: gather samples to model the distribution of a certain function.
- Approximate a quantity: e.g. the mean or variance value of a distribution.
- Optimize a function: define a sample that maximizes or minimizes the target function

When planning the energy dispatch of electrical distribution networks MC sampling is used to capture uncertainties on renewable power generation (e.g. PVs and wind turbines) or electric load demand. When modelling multiple uncertain parameters, MC will randomly sample every parameter and then create scenarios, which will be vectors containing one sampled value for every considered uncertainty.
The only requirement needed for MC methods to run is knowing the probability distribution of the uncertainty. When performing a general model, a normal distribution is typically chosen. In our work, uncertainties are assumed to have normal distributions with different standard deviations according to the underlying nature of the parameter.

In stochastic programming, the MC sampling technique is used not only when we need to generate a discrete number of uncertainty realizations, which are necessary to solve the problem itself, but also when performing feasibility checks. Indeed, it is common practice to test the optimal solution found on a large set of scenarios so that its robustness can be evaluated. Another set of new scenarios will then be generated, having approximately the same size as the previous initial set. Thus, the feasibility rate of the optimal solution will be given by the ratio between the number of feasible solutions determined and the size of the test scenario set.

4.3.2 Simultaneous backward reduction

The MC simulation will generate a large number of scenarios subject to the defined probability distribution. The probability given to each scenario will be equal to one divided by the number of the sampled scenarios. As previously mentioned, to better approximate uncertainties we have to increase the number of sampled scenarios. Unfortunately, this will result in our model having a very high computational burden, hence requiring the set of scenarios to be reduced. In this thesis, an efficient algorithm based on *simultaneous backward reduction* was used [44]. The purpose of this

technique is to determine a representative subset of scenarios and their probabilities so that the reduced subset will best represent the initial distribution. Wu's *et al's* method aggregates most similar scenarios by measuring a distance of probability distribution as a probability metric until the target subset dimension is reached.

Let $\Omega_s = \{\omega_1, \dots, \omega_K\}$, with $s = (1, \dots, K)$ be the initial scenario set containing *K* initial scenarios, each of them having a probability ρ_s. The probability distance between two scenarios $(s, \dot{s})$ is given by:

$$d_{s,\dot{s}} = \max\left\{1, || s - \overline{s} ||, || \dot{s} - \overline{s} ||\right\} || s - \dot{s} || \qquad 4.13$$

where $\overline{s}$ is the average value of scenarios.

Let S be the initial set of scenarios and J the set of scenarios to be deleted (initially null). The simultaneous backward reduction method includes the following steps:

Step 1: Compute the distances of all scenario pairs $d_{s,\dot{s}} = d(\omega_s, \omega_{\dot{s}})$, with s, $\dot{s} = 1, \dots, K$.

Step 2: For each scenario k, $dt_k(r) = \min d_{k,\dot{s}}$, $\dot{s}, k \in S$ and $\dot{s} \neq k$ and r is the scenario index that has the minimum distance with scenario k.

Step 3: Compute $\rho d_k(r) = \rho_k \times dt_k(r), k \in S$. Choose d so that $\rho d_d = \min \rho d_k, k \in S$.

Step 4: $S = S - \{d\}$, $J = J + \{d\}$; $\rho_r = \rho_r + \rho_d$.

Step 5: Repeat steps 2-4 until the number of scenarios to be deleted meets the request.

After reducing the set of scenarios to the desired size, this set is going to be formed by the most representative scenarios, hence eliminating those scenarios too similar to each other. By reducing the number of scenarios we are also reducing the accuracy of the uncertainty model.

4.4 **Optimization Solvers**

In this thesis work, the model built upon Chapter 2 and Chapter 3 formulations represents a *mixed-integer linear programming* problem (MILP). All constraints are written in a linear form, while the variables used are both stated in continuous and binary form, thus making the problem *mixed*. Simulations are conducted on a 64-bit PC with 2.80-GHz CPU and 16 GB RAM using MATLAB platform.

The proposed model is implemented in the YAMILP platform [45], which allows the problem to be built within a MATLAB interface, and solved thanks to GUROBI solver [46], one of the most used commercial solvers for linear and quadratic programming.

CHAPTER 5
TEST SYSTEM DESCRIPTION

5.1 **MEMG System**

5.1.1 **Network topology**

The topology of both the microgrid and the district heating considered in this thesis comes from the *14-Bus Radial System* introduced by Basu *et al* [47]. A representation of the microgrid layout is shown in Fig. 5.1, while both supply and return pipelines of the district heating are shown in Fig. 5.2 with red and blue colors, respectively.

Both MG and DH operate in *grid-connected* mode, which allows them to exchange power/heat with the upstream transmission systems. Thus, when costumers' demand cannot be fulfilled, the MEMG operator purchases power/heat from the transmission system operator (TSO). When the available power/heat in the MEMG exceeds the costumers' request instead, the MEMG operator sells back to the TSO.

Although the nature of the upstream systems feeding the MEMG is kept general, an assumption regarding power and thermal slack buses was made, following [15] approach. This is to say that the power and thermal slack buses are supposed to be connected to transmission system buses whose power and heat flows are not dependent on one another; in other words, the power and heat exchanged from upstream must not

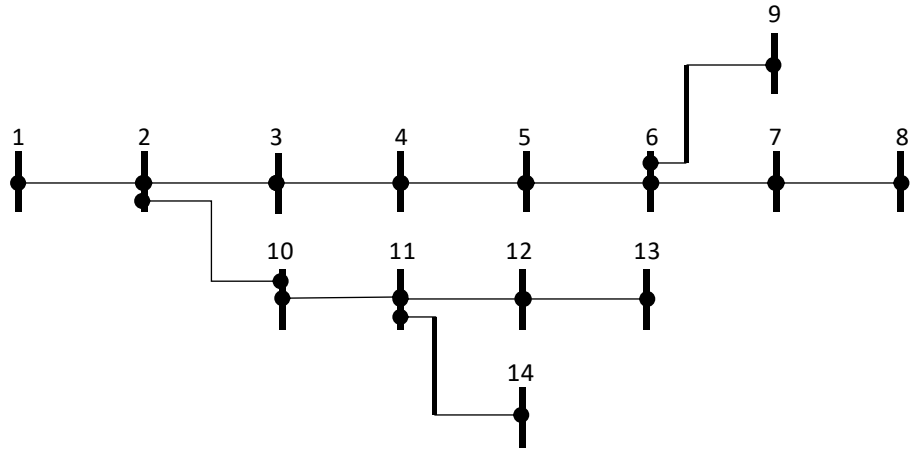

Fig. 5.1 One-line diagram of the 14-bus radial system

be proportional to each other. Therefore, for example, the two slack buses cannot be fed by the same cogeneration plant (e.g. a CHP) - which would be able to compensate MEMG unbalances - but they could be connected to two different CHP.

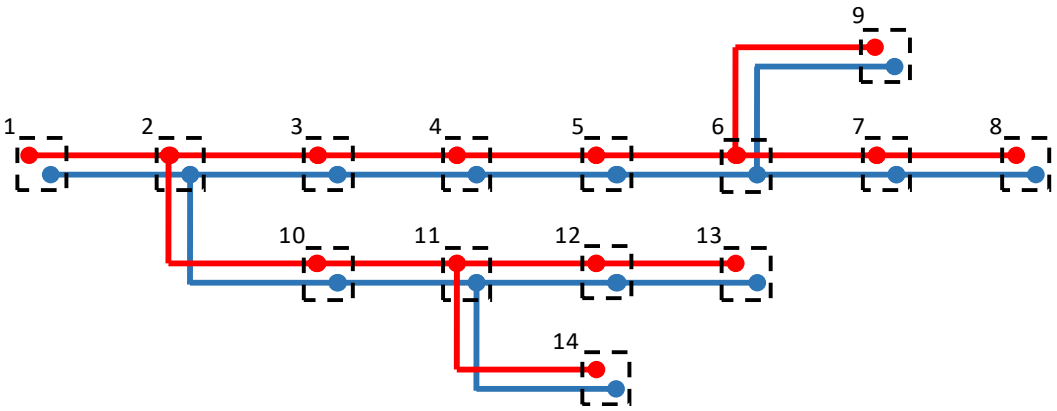

Fig. 5.2 District heating supply and return networks

5.1.2 **Multi-Energy Device Allocation**

In Fig. 5.3, the structure of the MEMG considered in this case study is shown. As it can be observed, the MEMG can simultaneously supply electric and thermal energy to customers. Consequently, the MEMG operator must coordinate the energy flows of both energy vectors to satisfy customers' demand while meeting system constraints. From the electrical point of view, the MEMG operator manages the power output of CHP units and PV panels distributed along the system. Since PVs output generation depends on the irradiance profile of the considered day, and because no electric storage units are provided, CHP units must be controlled so that PVs fluctuations do not destabilize the MG. From the thermal point of view instead, the MEMG operator manages the output heat produced by CHP units and SCs. Besides, all thermal units are equipped with a water-tank HST, which gives the MEMG operator more flexibility in the energy dispatch. Enabling heat energy to be stored allows CHP units not to be subjected to control strategies (cfr 3.3) and SCs to decouple their output from sun irradiance profile.
As previously mentioned, when energy balance cannot be found within the MEMG components, power and heat can be exchanged through the slack buses. In the electric and thermal substations, an MT/BT transformer and a heat exchanger are supposed to be placed, respectively.

In Table 5.1 the typology of components connected to each bus of the test case study is shown.

Table 5.1 Typology of components installed in the case study MEMG

Components	**Bus, *i***													
	1	**2**	**3**	**4**	**5**	**6**	**7**	**8**	**9**	**10**	**11**	**12**	**13**	**14**
PV panel			✓			✓			✓	✓			✓	
CHP								✓						✓
Solar collector				✓					✓	✓			✓	
Storage				✓				✓	✓	✓			✓	✓

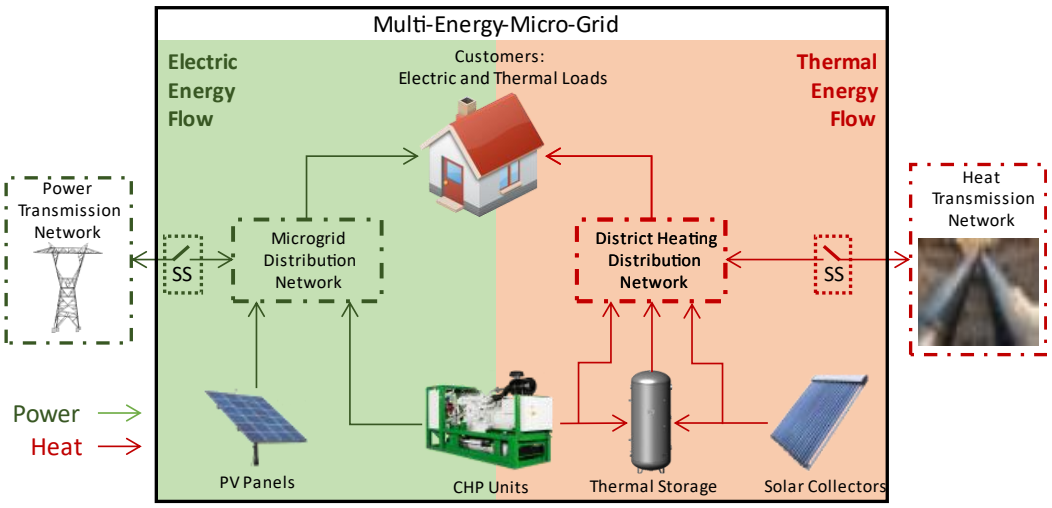

Fig. 5.3 Structure of the case study MEMG

It should be noticed that while the PVs and SCs positioning did not follow any particular consideration, CHP units were placed on the end-buses to help to maintain voltages across the system within an acceptable range. The further the buses are from the slack bus and the higher the voltage drop will be. Therefore, controlling the output active power of CHP units, allows the MEMG operator not only to compensate the severe PV output variations but also the strengthen up the weakest buses of the MG.

5.2 Parameters

5.2.1 Network parameters

The following tables show the values of MEMG network considered in this thesis work. Table 5.2 shows the electric slack bus parameters, while Table 5.3 lists the impedance of the *14-Bus Radial System* branches used in [47].
It is worth noticing that if an upstream OLTC is considered, the slack bus voltage V_0 could be defined as a state variable, thus adjusting its value according to the voltage fluctuations. This could be implemented in a future development of this model.

Table 5.4 shows the DH parameters and the upper and lower temperature bounds on each bus. Lastly, Table 5.5 lists the overall heat transfer coefficient of the DH pipelines.

Table 5.2 Electric slack bus parameters

Parameter	Value	Unit
v_0	1.05	p.u.
ε^{up}	0.05	p.u.
ε^{down}	0.15	p.u.
$P^{slack,\max}$	1	MW
P^{cap}	300	kW

Table 5.3 Branches impedance

Starting Bus, *i*	Ending Bus, *i*	*R* (Ω)	*X* (Ω)
1	2	0.0119	0.0414
2	3	0.0119	0.0414
3	4	0.0135	0.0421
4	5	0.0167	0.0845
5	6	0.0194	0.0592
6	7	0.0224	0.1200
7	8	0.0318	0.0845
6	9	0.0342	0.1704
2	10	0.0167	0.0420
10	11	0.0194	0.0592
11	12	0.0670	0.1710
12	13	0.0950	0.1989
11	14	0.0813	0.1558

Table 5.4 District heating parameters

Parameter	Value	Unit
$q^{slack,\max}$	1	MW
c_w	4.186	kJ/(kg °C)
L_i	400	m
$T^{s,\max}$	95	°C
$T_i^{s,\min}$	70	°C
$T_i^{r,\max}$	65	°C
$T_i^{r,\max,source}$	110	°C
$T_i^{r,\min}$	50	°C

Table 5.5 Pipelines overall heat transfer coefficients

Starting Bus, *i*	Ending Bus, *i*	λ W/(m K)
1	2	3
2	3	2
3	4	6
4	5	3
5	6	2
6	7	6
7	8	2
6	9	3
2	10	6
10	11	3
11	12	2
12	13	6
11	14	3

5.2.2 **PV and SC parameters**

Table 5.6 shows the PV installed capacity across the system, while Table 5.7 lists the SC parameters assumed in this thesis work.

In order to obtain the hourly contribution of both power and heat produced throughout the day, both Eq. 2.12 and Eq. 3.12 use the irradiance percentage profile G_{index}. The irradiance profile of 15th December 2019 in Lampedusa was extracted from the PVGIS database [48] and it is reported in Fig. 5.4.

Table 5.6 PV installed capacity

Bus,i	P^{PV} **(kW)**
3	30
6	30
9	10
10	10
13	10

Table 5.7 SC parameters

Parameter	***Value***	***Unit***
n_p	8	-
T_m	10	°C
$q^{sol,\max}$	1.08	kW

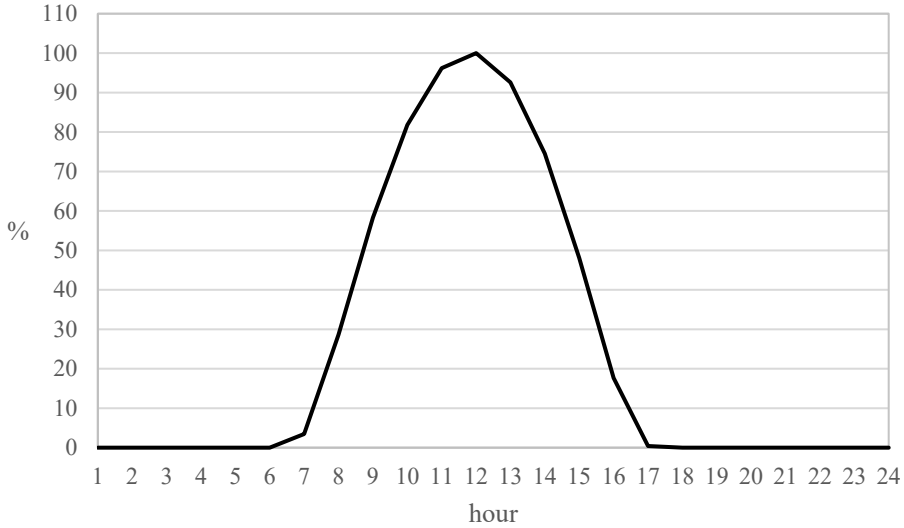

Fig. 5.4 Irradiance index of 15th January

5.2.3 **CHP and storage parameters**

Table 5.8 shows the CHP parameters used for the simulations, while in Table 5.9 the heat storage parameters of both SCs and CHPs are listed. In addition, the values

used for the self-discharging and charging/discharging efficiencies are η_{TS}= 0.95 and $\eta_{TSC/D}$= 0.97 respectively.

Table 5.8 CHP parameters

Parameter	Value	Unit
$P^{CHP,\max}$	160	kW
$P^{CHP,\min}$	16	kW
$H^{CHP,\max}$	300	kWh
$H^{CHP,\min}$	22.7	kWh
σ	9.78	kWh/m^3
η_{PGU}	0.33	-
η_{HR}	0.7	-
$ramp_{up}^{CHP}$	0.5	-
$ramp_{down}^{CHP}$	0.5	-

Table 5.9 Thermal storage parameters

Bus, i	$H^{TS,\max}$**(kWh)**	$H^{TSC/D}$**(kWh)**
4	400	50
8	400	50
9	300	37.5
10	400	50
13	300	37.5
14	400	50

5.2.4 **Load parameters**

Table 5.10 lists the base values of electric loads, which also come from Basu's work [47].

Table 5.10 Electric loads base value

Bus, i	P^L **(kW)**	Q^L **(kVar)**
2	20	6.5
3	85	27.9
4	40	13.1
5	20	6.5
6	20	6.5
7	7.6	1.6
8	10	3
9	6.1	1.6
10	11.2	7.5
11	61	9
12	1.6	6.1
13	9.0	5.9
14	13.5	6.1

In order to find the hourly values of the electric loads during the day, the base values

shown in Table 5.10 must be multiplied by the load index profile $load_{index}$ (cfr Eq. 2.19). The electric load profile of 15th January 2019 found on the website of the Italian TSO (Terna) [49] is shown in Fig. 5.5.

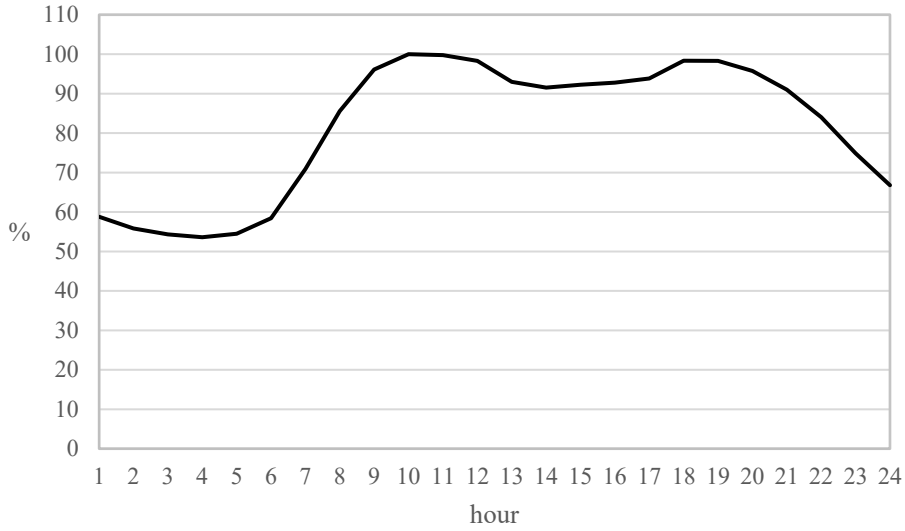

Fig. 5.5 Load index profile of 15th January

The customer's thermal load demand was modeled using the parameters listed in Table 5.11

Table 5.11 Thermal load parameters

Parameter	Value	Unit
$nb - n° \, buildings$	7	-
$nf - n° \, floors$	2	-
R	2.582	°C/kW
c_{air}	0.42	kWh/°C

As previously mentioned in Subsection 3.4.2, the heat load demand depends on the outdoor temperature values, which defines the *space heating* component. In this

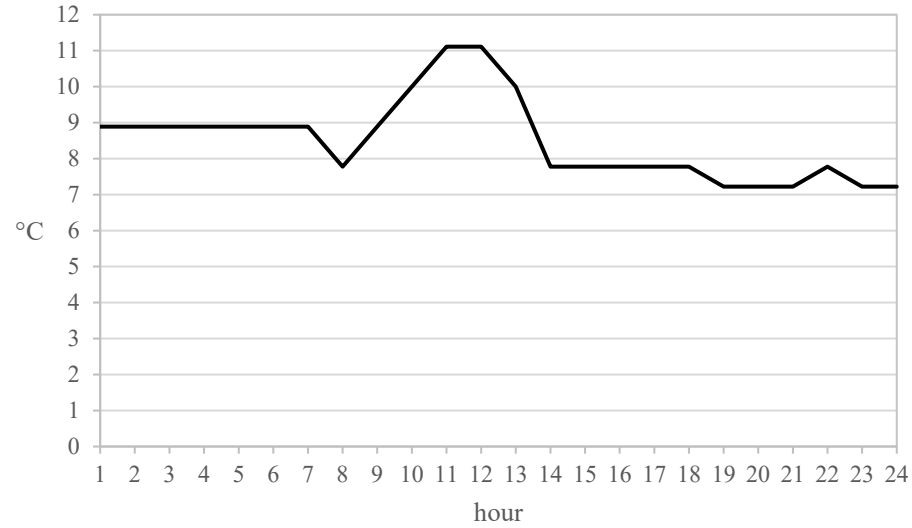

Fig. 5.6 Temperature profile of 15th January

thesis the temperature profile of Lampedusa on January 15th, 2019 was extracted from the Wunderground website [50]. Its profile can be seen in Fig. 5.6.

5.2.5 **Economic parameters**

The values of the parameters used to define the objective functions expressed by Eq. 4.5 and Eq. 4.12 are listed in Table 5.12.

Table 5.12 Cost components parameters

Parameter	Value	Unit
C^{fuel}	0.05	$/m^3
C^{CHP}	0.008	$/kWh
C^{PV}	0.012	$/kWh
C^{SC}	0.015	$/kWh
$C^{buy,el}$	0.07	$/kWh
$C^{sell,el}$	0.015	$/kWh
$C^{buy,th}$	0.14	$/kWh
$C^{sell,th}$	0.03	$/kWh
Pr^{el}	0.222	$/kWh
Pr^{th}	0.444	$/kWh

5.3 **Uncertainty Modelling**

As extensively explained in Chapter 4, to run stochastic optimization problems, uncertainties must be modeled upon their probability distribution curves. Also, to reflect the uncertainty probability distribution accurately, a large number of uncertainty scenarios need to be generated.

In this thesis work, all three types of uncertainty were assumed to follow the normal distribution where the mean values are those used in the deterministic problem (i.e. the

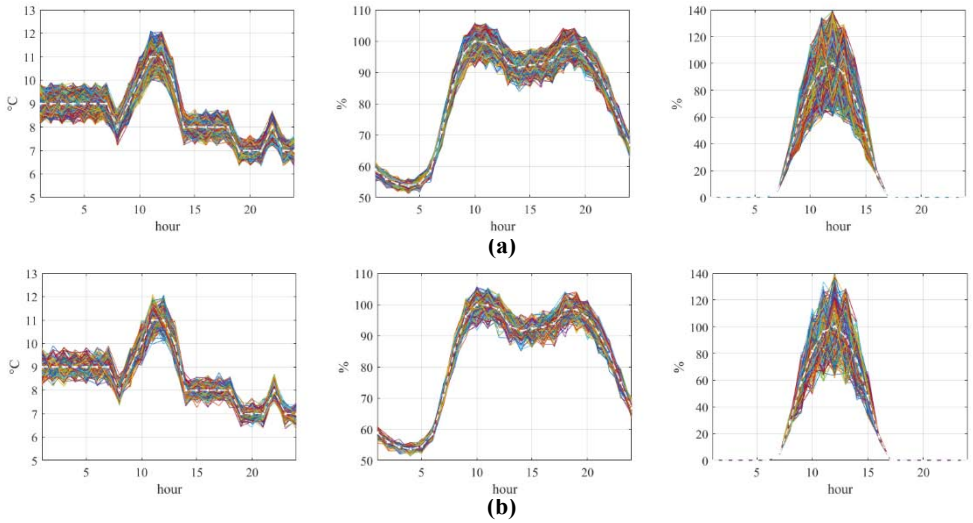

Fig. 5.7 a) initial generated sets of scenarios and b) reduced sets of scenarios. The white-dashed line represents the mean values

values shown in Fig. 5.4, Fig. 5.5, and Fig. 5.6). In particular, the electric load, the outdoor temperature, and the sun irradiation were supposed to have standard deviations equal to 3%, 5%, and 30%, respectively.
Then, the Monte Carlo sampling technique was used to build an initial set of 2000 uncertainty realizations (i.e. scenarios). To reduce the computing burden, simultaneous backward reduction (cfr 4.3.2) was used to reduce the scenario set to the most representative 200 scenarios. Fig. 5.7a shows the initial set of 2000 scenarios for the three uncertainties, while Fig. 5.7b shows the 200 reduced scenarios selected.

One important thing that must be highlighted is that the sun irradiation uncertainty acts differently on the PV and SC output generations, thus calling for the creation of two different scenarios.

As it was mentioned when explaining the PV and SC model, the underlying nature of the coefficient multiplying the G_{index} vector is different: in the first case, $P^{PV,\max}$ represents the electrical installed capacity, which can never be exceeded; in the second case $q^{sol,\max}$ represents the estimated maximum heat produced using the deterministic irradiance profile.

Because of the uncertainty deviations, generated irradiance scenarios might have some values above 1 (i.e. 100%), thus making the output power/heat greater than $P^{PV,\max}$ and $q^{sol,\max}$, respectively. However, while PV installed capacity represents an upper bound limit, SCs are not limited as such. Therefore, uncertainties must be treated differently and the former G_{index} uncertain parameter must be differentiated between:

- G_{index}^{SC}, which will be identical to the reduced scenarios.
- G_{index}^{PV}, whose values are equal to the reduced scenarios', except for those values greater than 1, which will be forced to 1.

To better understand what was just explained, Fig. 5.8 shows both G_{index}^{SC} and G_{index}^{PV} sets of scenarios.

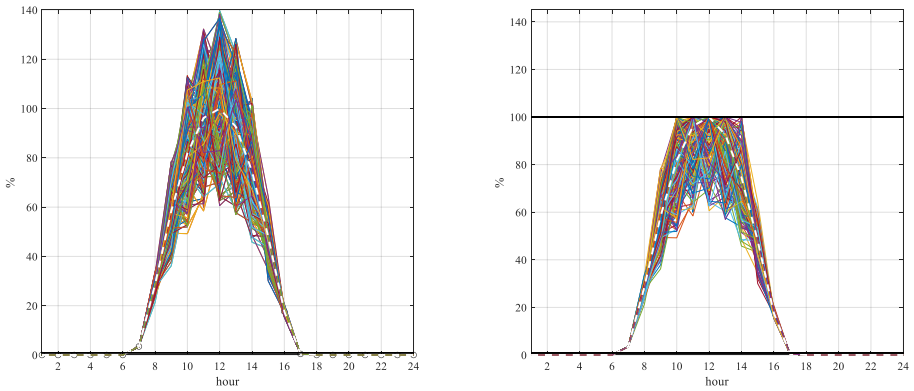

(a) **(b)**

Fig. 5.8 a) SC uncertainty scenarios and b) PV uncertainty scenarios
The white-dashed line represents the mean values

CHAPTER 6
NUMERICAL SIMULATIONS

6.1 Deterministic Results

As already extensively explained in the previous chapters, the deterministic optimization model solves the problem using the deterministic profiles of the uncertain parameters (i.e. the mean values of the normal probability distribution, Fig. 6.1).

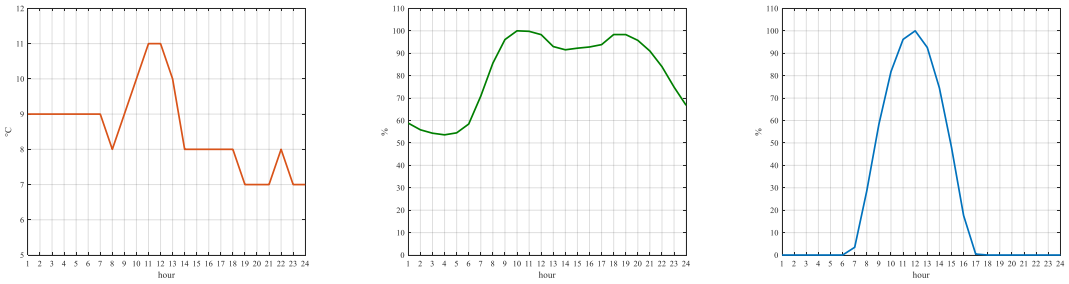

a) b) c)

Fig. 6.1 Profiles of the uncertain parameter: a) outdoor temperature, b) electric load and c) irradiance profile multiplier

Table 6.1 lists the realization of all cost terms considered in the deterministic objective function, which is rewritten below.

$$\min C_{CHP} + C_{OM} + C_{ex}^{el} + C_{ex}^{th} - C_{rev}^{el} - C_{rev}^{th}$$

Table 6.1 Cost terms of the determinist problem

Parameter	Value ($)
C_{CHP}	27.27
C_{OM}^{CHP}	14.08
C_{OM}^{PV}	6.50
C_{OM}^{SC}	21.83
C_{ex}^{el}	257.06
C_{ex}^{th}	1206.42
C_{rev}^{el}	1325.59
C_{rev}^{th}	2799.79
Net operating cost	2592.22

The values of both decision and state variables will be shown in the following subsections together with some considerations.

6.1.1 **Electric decision variables**

The solution found by the deterministic optimization problem gives the power output profiles in Fig. 6.2a. As it can be observed, the output power of both CHP at buses 8 and 14 remain approximately constant until 9:00 and 12:00, respectively. Then, both profiles decrease before ramping up to their peak power from 18:00 to 19:00. The output PV generation at buses 6 and 9, shown in Fig. 6.2b as representative buses with 30 and 10 kW capacity installed, follows the deterministic irradiance profile reaching their maximum values at 12:00.

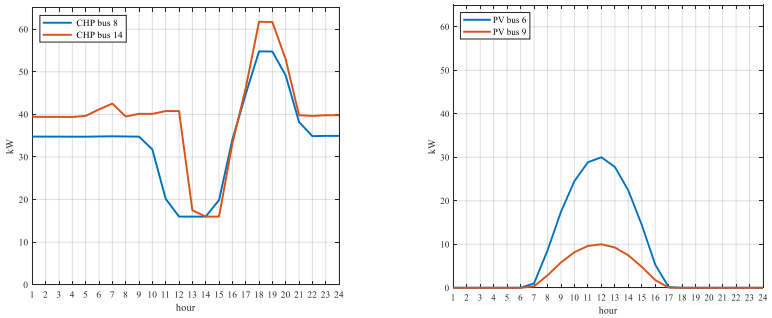

a) b)

Fig. 6.2 a) CHP output power in the deterministic case b) PV output power

To better understand the reason behind the CHPs dispatching profile, we can look at the system power balance in Fig. 6.3a, where the total CHP and PV contributions, together with the power withdrawn from the slack bus, are shown.

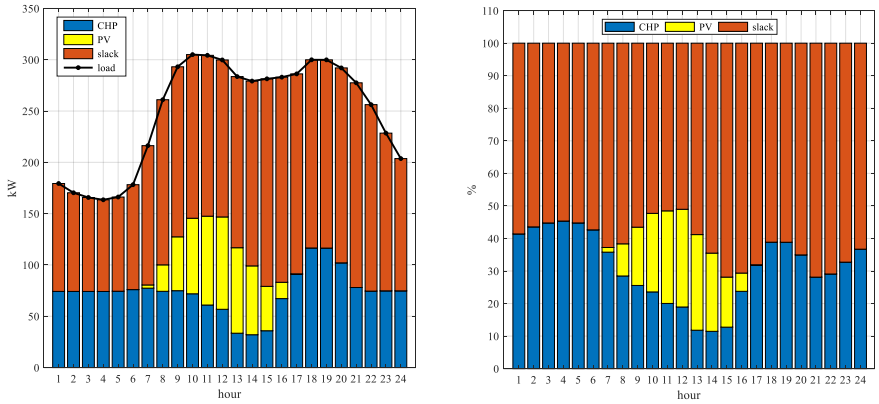

a) b)

Fig. 6.3 a) Electric distribution network power balance
b) Percentage contribution to load fulfillment

As can be seen, the MEMG power production follows approximately the load profile. In particular, the MEMG operator takes advantage of the PV production during the first load peak, hence reducing the contribution of the CHPs. Once the PV contribution starts fading away, CHP generation is ramped up to reduce the imported power from the slack bus during the second load peak from 18:00 to 19:00.

Another noteworthy piece of information can be extracted from Fig. 6.3b, where the percentage contribution of CHP, PV, and grid to the load fulfillment is shown. The

MEMG production covers around 40% of the total load demand thanks to the local generation, eventually surpassing 50% from 11:00 to 12:00.

6.1.2 **Voltage constraint**

When disconnecting the CHP units, the electrical and thermal distribution networks are uncoupled. This is because the MEMG is missing out the system coupling components, whose outputs influence both the power and thermal flow.

To appreciate the fundamental contribution of the CHP power output on the buses' voltages, Fig. 6.4a and Fig. 6.4b show the buses' voltage profile during the minimum and maximum load periods, respectively. While during the minimum load period voltages remain bounded within the allowable range (i.e. $0.9 \leq v_i \leq 1.1$), during the maximum load period the voltage on buses 5-9 and buses 12-14 falls below the minimum threshold. As it can be noticed, because buses 8 and 14 are among the buses more severely affected by the branches' voltage drop, these buses represent appropriate locations for placing CHPs.

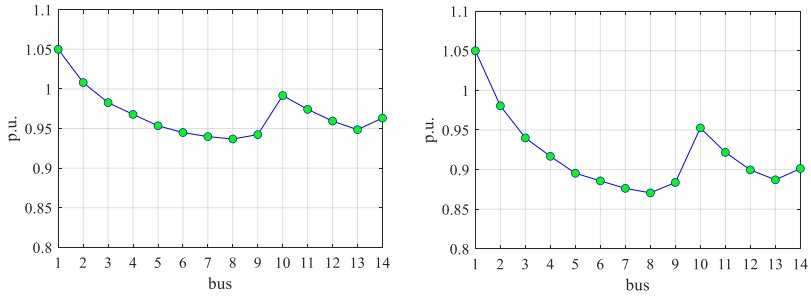

a) **b)**

Fig. 6.4 Voltages on buses during a) minimum load b) maximum load when CHP units are not considered

On the other hand, when CHP units are considered, the voltage constraint is respected during both minimum, Fig. 6.4a, and maximum load period, Fig. 6.4b.

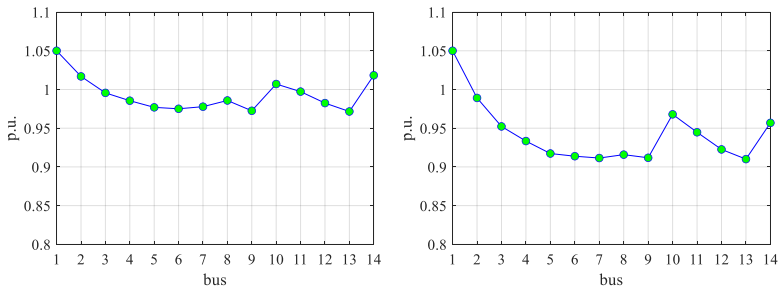

a) **b)**

Fig. 6.5 Voltages on buses during a) minimum load b) maximum load when CHP units are considered

In Fig. 6.6 the daily voltage profiles on three representative buses are shown. As we might have expected, all voltages are inversely proportional to the load. Indeed, all buses experience higher values at the beginning and at the end of the day, when the load is lower. Although not boldly evident, both PV and CHP buses show a ramping period during their peak generation.

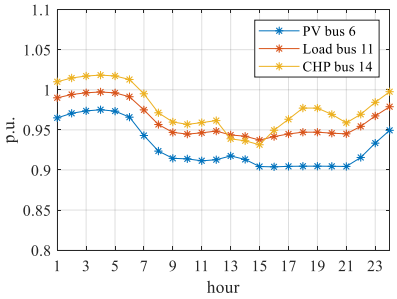

Fig. 6.6 Voltages on representative buses

6.1.3 **Electric system power balance**

During the day, the power produced by electrical generation units is used not only to alleviate the power demand on their own buses but also to inject power to the surroundings buses. This is obvious for the CHPs, whose main purpose is to feed the distribution network, Fig. 6.7a. Being the blue and black line the CHP generation and the load on the CHP bus respectively, only a small fraction (red area) is curtailed from the total power generated, dispatching all the rest (green area) to the MEMG. Similarly, bus 6 injects power to the distribution network when PV production exceeds the bus load demand Fig. 6.7b.

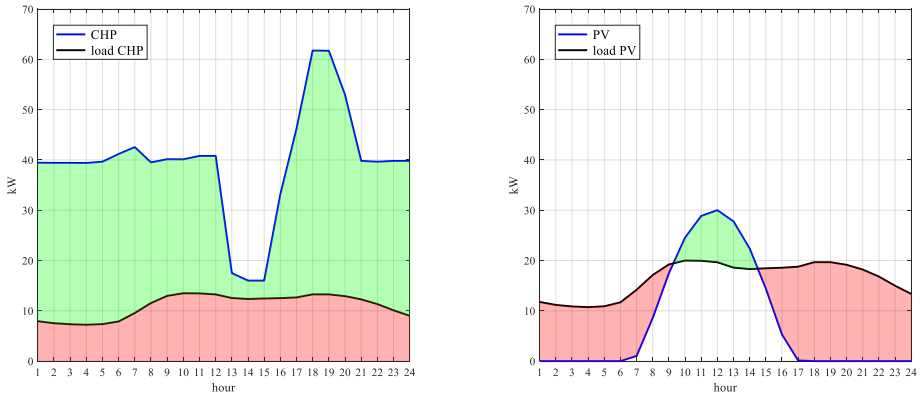

a) **b)**

Fig. 6.7 Generated power and load demand on bus a) 14 b) 6

6.1.4 **Thermal decision variables**

The optimal deterministic solution also defines the values of the thermal decision variables, i.e. the charging and discharging rates of the thermal storage and their initial State Of Charge (SOC). In order to evaluate the results, two reference buses were studied: bus 9 and bus 14 which host a SC and CHP unit, respectively. In Fig. 6.8 the storage dynamic of the representative buses is shown together with their heat production and SOC.

In Fig. 6.8a we can see that until 12:00 the heat production of the CHP is approximately constant and its HST only absorbs the amount of heat needed to compensate the self-discharging losses. As a result, the SOC remains fully charged until 12:00, when it starts diminishing due to the simultaneous reduction of output heat, reaching nearly 75%. At 15:00, the output heat starts ramping up until reaching its peak value from 18:00 to 19:00. At the same time, the HST charges back until reaching its

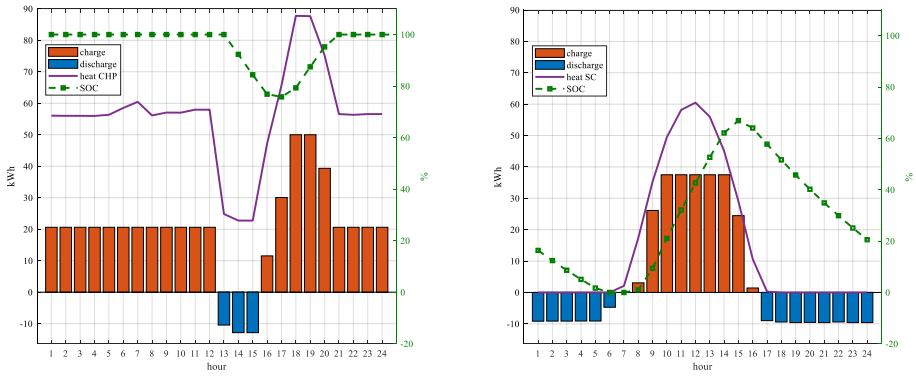

a) b)

Fig. 6.8 Storage dynamic and heat production (left axis) and SOC (right axis) of a) CHP at bus 14 and b) SC at bus 9

maximum capacity at 21:00. Again, from 21:00 to 24:00 the HST only absorbs the necessary heat to compensate the self-discharging losses.

In Fig. 6.8b instead, we can notice that the HST dynamic can be divided into three time intervals. In the morning, due to the lack of sun, the HST discharges from 1:00 to 6:00, going from having a 20% SOC to 0%. As the sun starts rising, and so the captured heat, the HST charges from 8:00 to 16:00, reaching a 68% SOC. After the sun is set, HST uses the stored heat to discharge back to the load, bringing the SOC to its initial value. It is worth noticing that at 7:00, when HST is emptied and the sun has not come up yet, the HST is not charging nor discharging.

6.1.5 **Temperature constraints**

Like the voltage constraint, the MEMG is subject to some temperature constraints. The blue line in Fig. 6.9a represents the total thermal load throughout the day, showing a minimum and a maximum demand at 5:00 and 21:00, respectively. As can be observed in Fig. 6.9b and Fig. 6.9c during both periods all temperatures across the pipeline distribution network are kept within the specified range of $70°C \leq T^s \leq 95°C$ and $50°C \leq T^r \leq 65°C$.

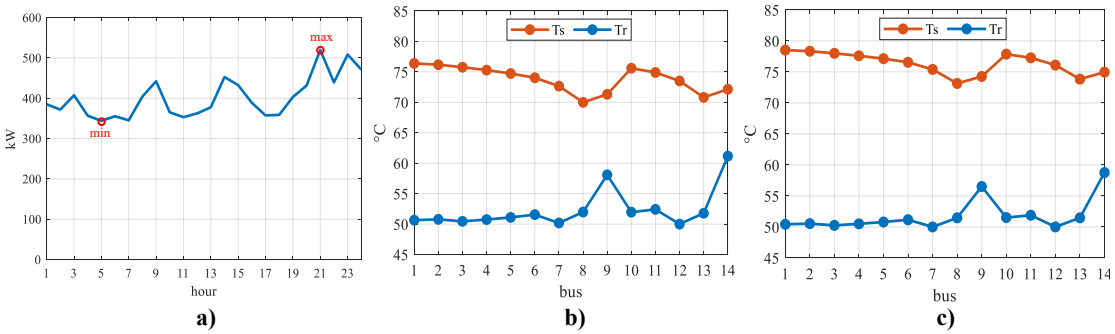

a) b) c)

Fig. 6.9 a) Total thermal load; supply and return temperatures on the network during b) minimum load and c) maximum load

Taking the already mentioned bus 9 and 14 as references, let's also consider bus 11 as a reference load bus. Fig. 6.10 shows that all supply, return and indoor temperatures are respectively within the prescribed range of $70°C \leq T^s \leq 95°C$, $50°C \leq T^r \leq 65°C$ (for passive buses), $50°C \leq T^r \leq 110°C$ (for active buses) and $16°C \leq T^i \leq 25°C$.

From Fig. 6.10a we can see that all supply temperatures follow the total load profile. Fig. 6.10b shows that setting a higher upper bound for active buses' return temperature allows the MEMG to reduce the heat withdrawn from the network, favoring the consumption of the distributed generation.

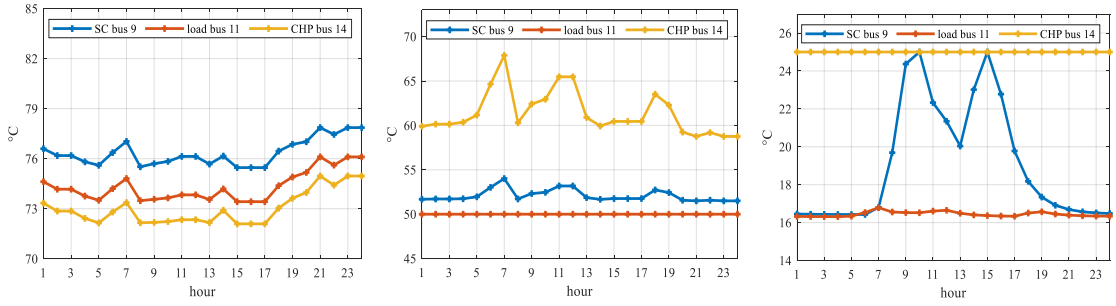

Fig. 6.10 Profile of a) supply, b) return, and c) indoor temperature

6.1.6 **Thermal energy injection analysis**

In Fig. 6.11 the thermal bus balances on the CHP and SC bus are shown, where all the heat contributions are shown to meet the load demand (black-dotted line). Fig. 6.12 represents instead all the possible flow distributions cases happening during the day.

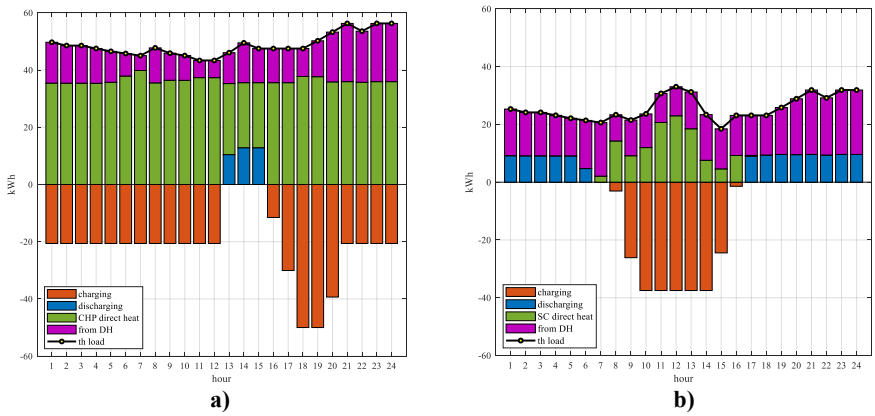

Fig. 6.11 Thermal node balance on a) CHP bus 14 and b) SC bus 9

As it can be observed, when scheduling the HST dynamic throughout the day, the optimization model allows the HST to absorb any amount of heat up to its maximum charging rate. Thus, when the produced heat exceeds the HST charging request, all the remainder goes directly to the thermal load, Fig. 6.12a. For the CHP bus, this happens from 1:00 to 12:00 and from 16:00 to 24:00. On the SC bus instead, this situation occurs from 8:00 to 16:00. In particular, from 10:00 to 14:00 the HST reaches its maximum charging rate, hence forcing all the remaining heat to the load.

During the CHP output drop, 13:00 – 15:00, the HST discharges, thus reducing the bus need for heat from the network, Fig. 6.12b. In the SC case instead, when the sun elevation does not allow any direct contribution, the load is met thanks to the HST discharged heat and the substantial support from the network, Fig. 6.12c.

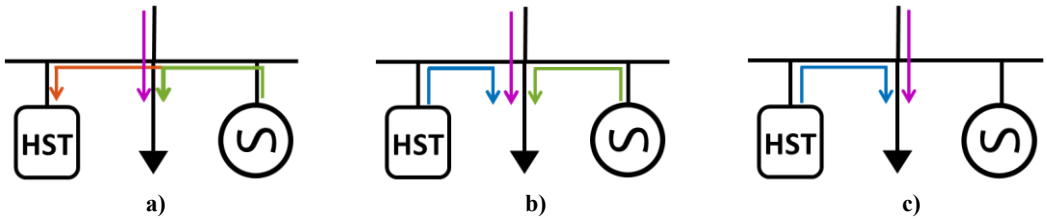

Fig. 6.12 Possible heat flow distributions on active buses

6.1.7 **Thermal system energy balance**

To verify the system's thermal balance, we must make sure that the system's thermal generation can fulfill the system's thermal load. Fig. 6.13 shows that, apart from the imported heat from the slack bus, the MEMG operator can count on the direct and discharged heat of both CHP and SC buses to match the thermal load and the network losses.

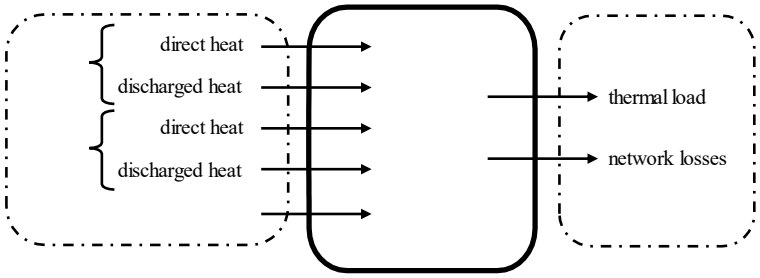

Fig. 6.13 System' thermal balance variables

By looking at the bar chart in Fig. 6.14, the first noticeable fact is that, different from the electrical system, from the thermal point of view the MEMG relies heavily on the imported heat from the upper-level transmission system. On average the MEMG local production covers 23% of the system load, reaching a maximum contribution of 36% at 9:00.

The combination of direct and discharged heat from the CHP buses makes their overall contribution constant throughout the day, injecting roughly 65 kWh on each timestep. Hence, the total thermal energy released by CHP buses amounts to 15% of the daily thermal demand.

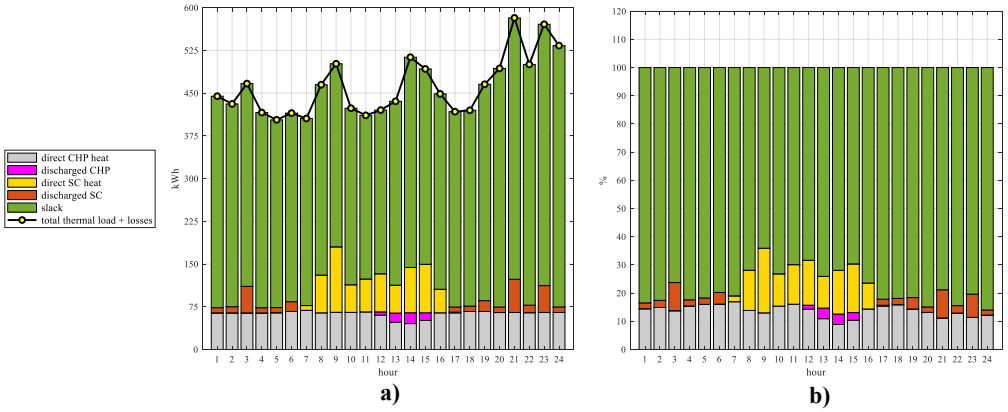

Fig. 6.14 System thermal balance in: a) absolute values and b) percentage

On the other hand, SC buses' contribution is concentrated mainly during the middle of the day, thanks to the direct heat component. The HSTs also support the system

generation discharging either in the morning and at night. The SC buses' contribution to the daily thermal demand amounts to 8%.

One last feature worth mentioning relates to the composition of the system's thermal load. In Fig. 6.15 it can be observed that space heating component represents the most relevant term, covering 75% of the overall system load, followed by the DHW term (14%) and network losses (12%). As it can be noticed, indoor temperature control term takes on negative values, meaning that the indoor temperature from one timestep to another has been changed.

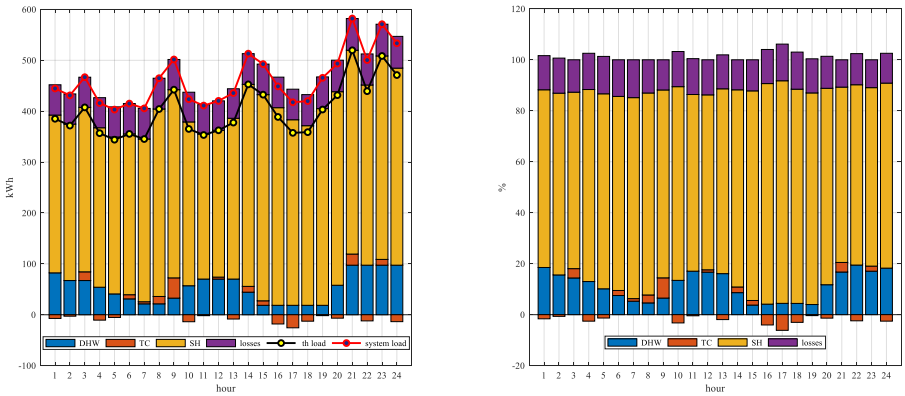

a) **b)**

Fig. 6.15 System thermal load in: a) absolute values and b) percentage

6.2 Stochastic Results

When looking for the optimum stochastic solution, the solver must find the set of decision variables that minimize the following objective function:

$$\min\ C_{CHP} + C_{OM}^{CHP} + \sum_{k=1}^{K} \rho_k \left[C_{OM,k}^{PV} + C_{OM,k}^{SC} + C_{ex,k}^{el} + C_{ex,k}^{th} - C_{rev,k}^{el} - C_{rev,k}^{th} \right]$$

Table 6.2 lists the CHP related cost terms together with the weighted summation of decision and scenario costs. Since all the cost terms related to state variables or uncertainties expectations are weighted by their respective probability density ρ_k, only the cost terms depending on the CHP output power can be compared with their respective deterministic equivalents. Both cost terms are slightly higher than the deterministic, meaning the CHP contribution is now a little bigger. The resulting net operating profit turns out to be a little lower than the deterministic, by only 10$, which is a penalty definitely worth to be paid for a much more reliable dispatch.

Table 6.2 Stochastic realized cost terms

Parameter	Value ($)
C_{CHP}	28.00
C_{OM}^{CHP}	14.45
C_{Σ}	2,625.37
Net operating cost	2,582.92

6.2.1 **Electric decision variables**

Let's now compare all the stochastic decision variables with their corresponding deterministic ones. In Fig. 6.16 the output profile of both CHP units on buses 8 and 14 are shown. From Fig. 6.16a we can notice that the stochastic output dispatch of the first CHP is significantly lower during the morning, but from 9:00 it stays moderately higher throughout the day. Instead, the second CHP generation falls below the deterministic output only from 11:00 to 13:00, before ramping up and reaching a much higher power peak, 90 kW.

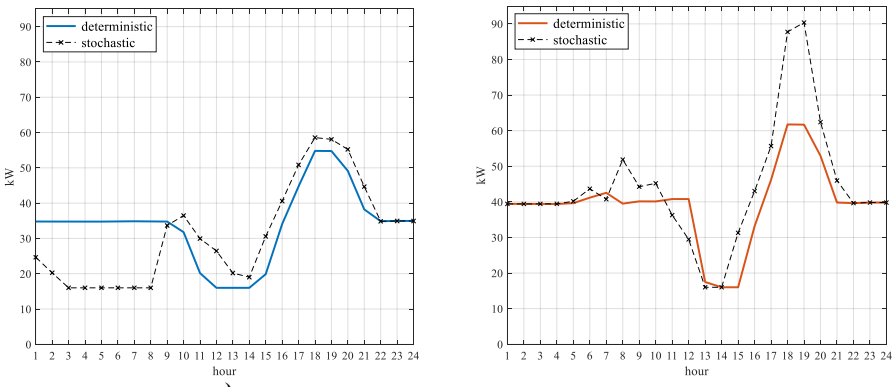

Fig. 6.16 Deterministic *vs* stochastic CHP output power on a) bus 8 and b) bus 14

6.2.2 **Voltage constraints**

To prove that the given stochastic solution can also satisfy the state variables constraints, the values of decision variables were applied to the deterministic model using the average uncertainty profiles (i.e. the deterministic scenario).

Starting from the voltage constraint, Fig. 6.17 demonstrates that all voltages during both minimum and maximum load periods are kept within the allowed range

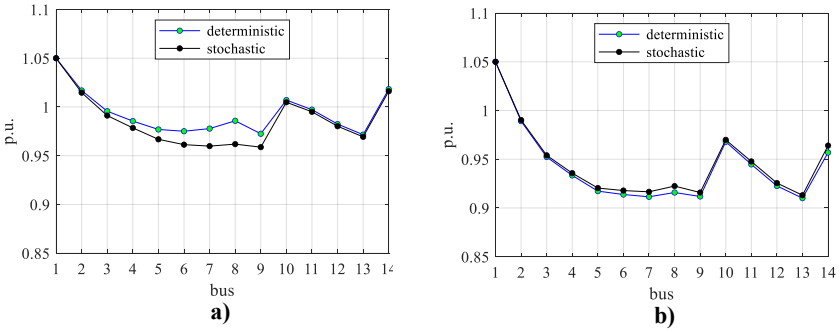

Fig. 6.17 Deterministic *vs* stochastic voltage profiles during a) minimum and b) maximum load periods

6.2.3 **Thermal decision variables**

In Fig. 6.18 the State Of Charge of the HST units on the CHP bu14 and SC bus are reported. As we can see, both profiles do not differ significantly from the deterministic. The CHP unit starts ramping down before than the deterministic, For this reason, it also starts charging back earlier. The SC instead, has a lower initial heat availability, so its

profile remains below the deterministic during all day. Also, from 6:00 to 8:00 the HST of the SC remains empty.

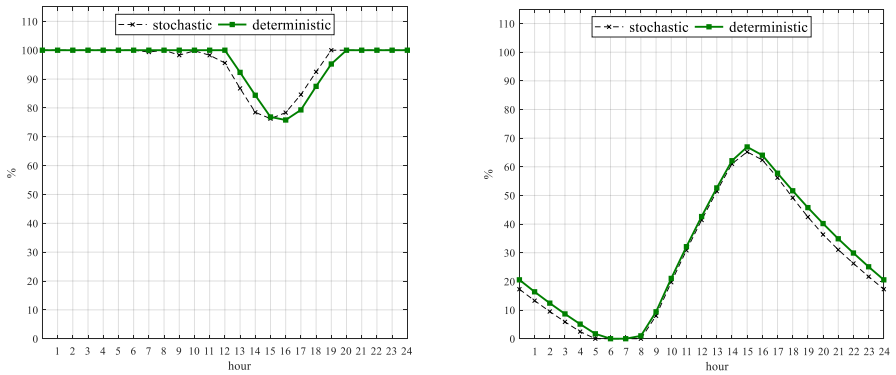

Fig. 6.18 Deterministic *vs* stochastic SOC of HST on a) CHP bus 14 and b) SC hus 9

To get a better understanding of the HSTs dynamic we can also look at the bar charts in Fig. 6.19. As we can see from Fig. 6.19a, the HST of the CHP behaves the same as the deterministic until 6:00, absorbing from the CHP only the heat needed to compensate the self-discharging losses. As previously observed in Fig. 6.18a we can notice that in the stochastic solution, the HST begins charging back one hour before the deterministic solution. Then again, from 21:00 until the end of the day, only the top-up heat is charged.

The HST of the SC follows approximately the same behavior of the deterministic solution. Fig. 6.19b allows us to appreciate clearly that from 6:00 to 8:00 the HST remains empty from with no heat charged nor discharged, as we noticed before in Fig. 6.18.

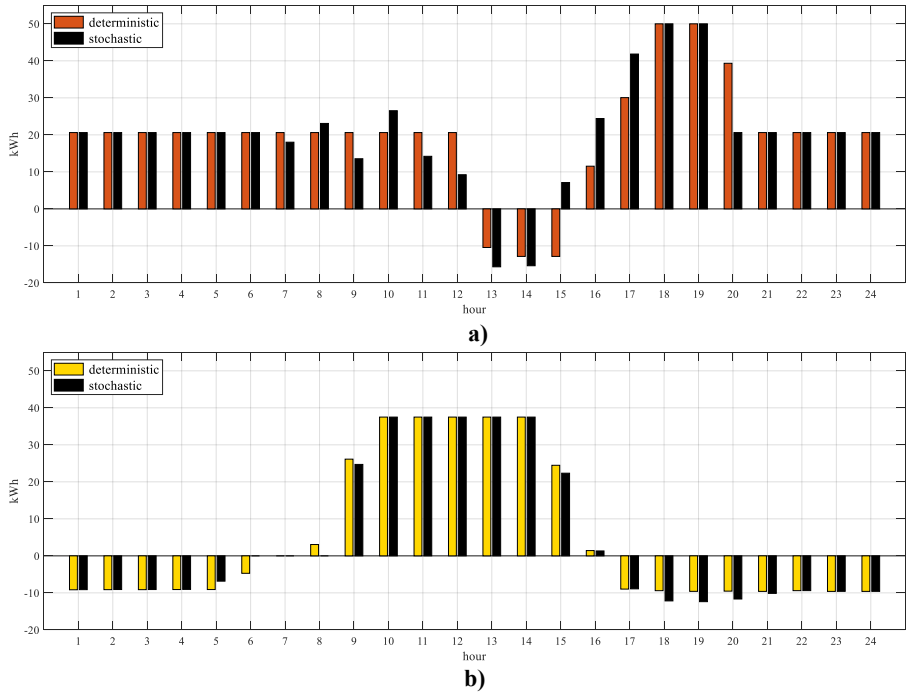

Fig. 6.19 Deterministic *vs* stochastic HST dynamic on a) CHP bus 14 and b) SC hus 9

6.2.4 **Temperature constraints**

Because the stochastic solution yields different decision variable values, both power and thermal flow differ from the deterministic case. Also, since the thermal load does not follow a predetermined profile, heavily depending instead on indoor temperatures, it is not surprising that its profile differs from the deterministic case. Fig. 6.20a shows that the stochastic solution determines a thermal load profile having a minimum and maximum peak at 4:00 and 23:00, respectively. Both supply and return temperatures of the distribution network are evaluated in the two representative load conditions. Fig. 6.20b and Fig. 6.20c show that all temperatures are within their constraint values, deviating almost imperceptibly from the stochastic profiles.

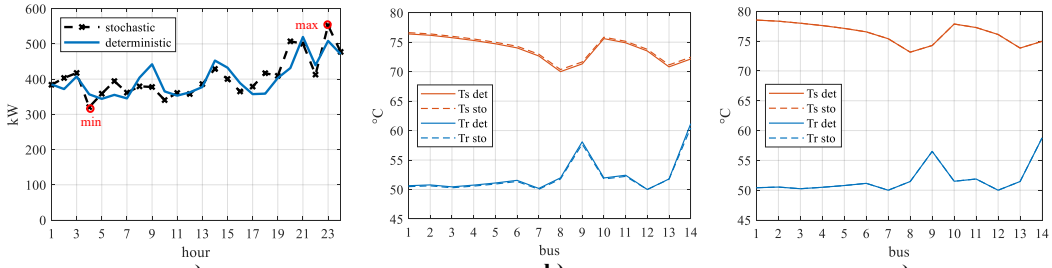

Fig. 6.20 Deterministic *vs* stochastic a) thermal load and supply and return temperatures during a) maximum and b) minimum load periods

Finally, the indoor temperatures on the three representative buses used in 736.1.5 are reported in Fig. 6.21. While the CHP bus profile stays almost the same, Fig. 6.21a, both SC and load profiles vary considerably throughout the day.

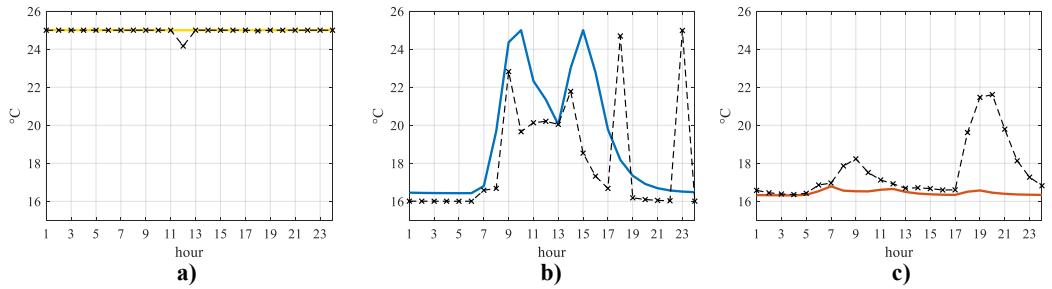

Fig. 6.21 Deterministic *vs* stochastic indoor temperature on representative a) CHP, b) SC and c) load bus

6.3 **Feasibility Check**

To test the robustness of the stochastic solution (SS), we carried out a feasibility check based on a large number of test scenarios. By testing the SS on a large number of different scenarios, we aim at evaluating the feasibility of our solution when different uncertainty realizations occur.

A second set of 2000 new scenarios was created using the Monte Carlo sampling technique. Then, the SS was tested on each scenario, hence solving 2000 different deterministic problems. While solving each of these deterministic problems, the number of scenarios whose constraints were not violated was counted. Finally, the feasibility ratio (FR) was calculated by doing the ratio between the number of feasible solutions

and the total number of test scenarios, i.e. 2000. In our case, the number of scenarios for which the SS determined constraint violations is equal to 175, which is 8.75% of all possible 2000 scenarios. This indicates that our solution does not only guarantee higher profits but also proves to be robust for a wide range of uncertainty realizations, thus increasing operating performances.

For a comprehensive analysis of how the uncertainty modelling impacts the problem solution, the stochastic optimization model was tested on uncertainty models based on different numbers of scenarios. The logic scheme of this feasibility analysis is shown in Fig. 6.22.

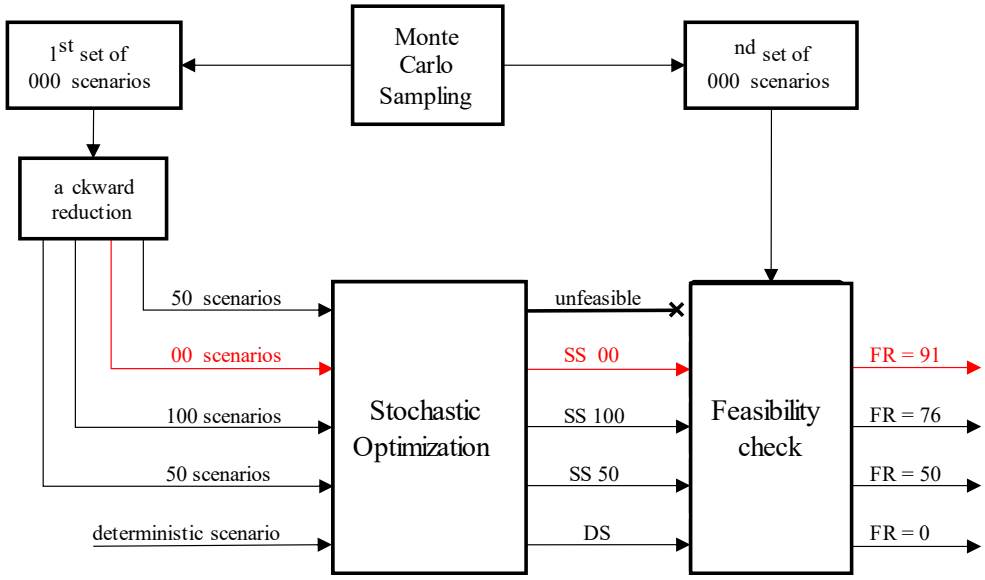

Fig. 6.22 Feasibility rate diagram

Each uncertainty model comes from applying the simultaneous backward reduction method to the first set of 2000 scenarios (i.e. the same scenario used to find our case study reduced 200 scenarios) with different target reduced scenarios. Each of these reduced scenario set was then used to solve our proposed stochastic optimization problem. Finally, every feasible solution found was used to solve each scenario of the second set of 2000 scenarios (i.e. the same scenarios test set used for the feasibility check of the 200 scenario-based SS). All the obtained results are reported in Table 6.3.

Table 6.3 Sensitivity analysis results

Number of scenarios	Solution time (min)	Optimum profit ($)	% profit increase vs Det	Average check profit ($)	Feasibility rate (%)
deterministic	0.07	2592.22	-	-	0
50	3.04	2586.59	0.22	2583.10	50
100	10.23	2584.03	0.32	2582.70	76
200	35.68	2582.92	0.36	2582.30	91
250	44.43	unfeasible	-	-	-

The first thing we notice is that the FR grows with the number of considered scenarios. Although the 50 scenario-based solution yields to only 50% of feasible scenarios, the FRs increase as the number of scenarios modelling the uncertain

parameters is enlarged. This shows how critical it is to choose an adequate number of scenarios when modelling uncertain parameters to guarantee the robustness of the problem solution.

Unfortunately, although higher robustness can be achieved increasing the number of considered scenarios, solving time increases significantly. By looking at the second column of Table 6.3 we can see that the solution time grows more than linearly with the number of considered scenarios, going from just 3 minutes in the 50 scenarios case up to 44 minutes in the 250 scenario case. As was to be expected, higher computational burden is the price we must pay for higher operation performances.

Regarding revenues of the MEMG operation, net operating profit slightly decreases with the number of considered scenarios. The same trend is shown when looking at the average profit of the 2000 deterministic problems of the feasibility check.

One last thing worth noticing relates to the last line of Table 6.3. When trying to solve the stochastic optimization problem with a 250 scenario-based uncertainty model, the solver could not find any solution, making the problem *unfeasible*.

CHAPTER 7
CONCLUSIONS AND FUTURE WORKS

This thesis introduced a method for operational optimization of Multi-Energy Microgrids when different types of uncertainties are considered. The day-ahead operation strategy is modeled as a single-stage stochastic optimization programming problem based on a MILP formulation; this allows our method to be efficiently implemented by commercial solvers. Compared with conventional deterministic MEMG day-ahead operation strategies, our model solution can guarantee optimal profits under stochastic variations of electric load, thermal load and RES output.

A feasibility check was carried out to test how the proposed method performs when different uncertainty realizations occur. The results demonstrated that the robustness of the stochastic operation method strongly depends on the accuracy of the uncertainty model. As the number of scenarios used to capture the uncertainty variability is increased, the robustness of the corresponding solutions increases accordingly. Thus, to guarantee reliable operation solutions, our stochastic method needs to be given uncertainty models based on a large number of scenarios. It is worth noticing that the higher the number of scenarios used, the higher the computational burden will be. Hence, the number of scenarios used should be the result of a trade-off between the solution robustness and the solving time required.
When modelling uncertainties upon 200 scenarios, the solution of the stochastic problem resulted to be feasible against 91% of 2000 random scenarios, hence proving very good robustness. The computing time was 35.7 minutes, which is fully compatible with day-ahead operation planning.

If this model was used for intra-day operation optimization, which requires much shorter solving time, a smaller number of scenarios could be used. Indeed, with a short lead time, energy uncertainties can be accurately forecasted (i.e. uncertainties have much lower standard deviations) and so the generated scenarios are not going to be too different from each other. This allows a smaller number of scenarios to be selected, thereby reducing computing time.

When solving the proposed stochastic method on a 250 scenarios-based uncertainty model, the solver could not find any solution, hence making the problem *unfeasible*. The root reason for this lies in the fact that the current single-stage operation

model cannot cover all scenarios, revealing the system robustness issues. This means that for the considered physical system, the current operation strategy will never allow a FR = 100%. To overcome this limit, two possible further developments could be implemented:

- *Modify the physical system*, which means acting on all the hardware components investing and installing in the system by future system updates and planning.
- *Modify the control strategy,* either introducing an adaptive recourse action, real-time local control or advanced model predictive control.

In practice, hardware updates are often non-viable. This is because of the high investment costs involved in installing new equipment, which investors always try to limit. Hence, investing in a control strategy improvement is preferred.

Another development could be to overcome the limit of the underlying programming technique used. Indeed, stochastic programming can be implemented only when uncertainty probability distribution is known. In future works, programming techniques not requiring pre-defined distribution could be investigated.

REFERENCES

[1] "EEA greenhouse gas - data viewer," *European Environment Agency*. https://www.eea.europa.eu/data-and-maps/data/data-viewers/greenhouse-gases-viewer.

[2] Anonymous, " 030 climate & energy framework," *Climate Action - European Commission*, Nov. 23, 2016. https://ec.europa.eu/clima/policies/strategies/2030_en.

[3] Z. Zhou, J. Zhang, P. Liu, Z. Li, M. C. Georgiadis, and E. N. Pistikopoulos, "A two-stage stochastic programming model for the optimal design of distributed energy systems," *Appl. Energy*, vol. 103, pp. 135–144, Mar. 2013, doi: 10.1016/j.apenergy.2012.09.019.

[4] Cuo Zhang, Y. Xu, ZhaoYang Dong, and Jin Ma, "A composite sensitivity factor based method for networked distributed generation planning," in *2016 Power Systems Computation Conference (PSCC)*, Genoa, Italy, Jun. 2016, pp. 1–7, doi: 10.1109/PSCC.2016.7540822.

[5] K. Zou, A. P. Agalgaonkar, K. M. Muttaqi, and S. Perera, "An Analytical Approach for Reliability Evaluation of Distribution Systems Containing Dispatchable and Nondispatchable Renewable DG Units," *IEEE Trans. Smart Grid*, vol. 5, no. 6, pp. 2657–2665, Nov. 2014, doi: 10.1109/TSG.2014.2350505.

[6] C. Zhang, Y. Xu, Z. Y. Dong, and K. P. Wong, "Robust Coordination of Distributed Generation and Price- ased Demand Response in Microgrids," *IEEE Trans. Smart Grid*, vol. 9, no. 5, pp. 4236–4247, Sep. 2018, doi: 10.1109/TSG.2017.2653198.

[7] "EU solar boom: over 100 solar market increase in 019." https://www.solarpowereurope.org/eu-solar-boom-over-100-solar-market-increase-in-2019/.

[8] K. Turitsyn, P. Šulc, S. ackhaus, and M. Chertkov, "Distributed control of reactive power flow in a radial distribution circuit with high photovoltaic penetration," in *IEEE PES General Meeting*, Minneapolis, MN, Jul. 2010, pp. 1–6, doi: 10.1109/PES.2010.5589663.

[9] "Directive 004/8/EC of the European Parliament and of the Council of 11 February 004." https://eur-lex.europa.eu/legal-content/EN/ALL/?uri=CELEX%3A32004L0008.

[10] S. Martinez, G. Michaux, P. Salagnac, and J.-L. o uvier, "Micro-combined heat and power systems (micro-CHP based on renewable energy sources," *Energy Convers. Manag.*, vol. 154, pp. 262–285, Dec. 2017, doi: 10.1016/j.enconman.2017.10.035.

[11] A. Padovan and D. Del Col, “Solar thermal systems,” Università degli Studi di Padova.
[12] “PIANO NAZIONALE INTEGRATO PER L’ENERGIA E IL CLIMA.” https://www.mise.gov.it/images/stories/documenti/PNIEC_finale_17012020.pdf.
[13] P. Mancarella, “MES multi-energy systems): An overview of concepts and evaluation models,” *Energy*, vol. 65, pp. 1–17, Feb. 2014, doi: 10.1016/j.energy.2013.10.041.
[14] H. Zhao, *Analysis, Modelling and operational optimazation of district heating systems*. Centre for District Heating Technology, 1995.
[15] X. Liu, J. Wu, N. Jenkins, and A. agdanavicius, “Combined analysis of electricity and heat networks,” *Appl. Energy*, vol. 162, pp. 1238–1250, Jan. 2016, doi: 10.1016/j.apenergy.2015.01.102.
[16] D. Rutz, C. Winterscheid, and T. Pauschinger, “Upgrading the performance of district heating networks.” WIP Renewable Energies, Munich, Germany, 019.
[17] A. Messac, *Optimization in practice with MATLAB for engineering students and professionals*. New York, NY: Cambridge University Press, 2015.
[18] “Introduction to Optimization | NEOS.” https://neos-guide.org/content/optimization-introduction.
[19] “Optimization Taxonomy | NEOS.” https://neos-guide.org/content/optimization-taxonomy.
[20] U. Derigs, *OPTIMIZATION AND OPERATIONS RESEARCH – Volume I*. EOLSS Publications, 2009.
[21] P. Fiorentin, *Teoria della misurazione*. Università degli Studi di Padova.
[22] H.-G. Yeh, D. F. Gayme, and S. H. Low, “Adaptive VAR Control for Distribution Circuits With Photovoltaic Generators,” *IEEE Trans. Power Syst.*, vol. 27, no. 3, pp. 1656–1663, Aug. 2012, doi: 10.1109/TPWRS.2012.2183151.
[23] M. aran and F. F. Wu, “Optimal sizing of capacitors placed on a radial distribution system,” *IEEE Trans. Power Deliv.*, vol. 4, no. 1, pp. 735–743, Jan. 1989, doi: 10.1109/61.19266.
[24] C. Zhang, Y. Xu, Z. Li, and Z. Y. Dong, “Robustly Coordinated Operation of a Multi-Energy Microgrid With Flexible Electric and Thermal Loads,” *IEEE Trans. Smart Grid*, vol. 10, no. 3, pp. 2765–2775, May 2019, doi: 10.1109/TSG.2018.2810247.
[25] K. asar an, N. S. Cetin, and S. orekci , “Energy management for on-grid and off-grid wind/PV and battery hybrid systems,” *IET Renew. Power Gener.*, vol. 11, no. 5, pp. 642–649, Apr. 2017, doi: 10.1049/iet-rpg.2016.0545.
[26] T. Ma, H. Yang, and L. Lu, “A feasibility study of a stand-alone hybrid solar–wind–battery system for a remote island,” *Appl. Energy*, vol. 121, pp. 149–158, May 2014, doi: 10.1016/j.apenergy.2014.01.090.
[27] Z. Li, W. Wu, J. Wang, . Zhang, and T. Zheng, “Transmission-Constrained Unit Commitment Considering Combined Electricity and District Heating Networks,” *IEEE Trans. Sustain. Energy*, vol. 7, no. 2, pp. 480–492, Apr. 2016, doi: 10.1109/TSTE.2015.2500571.
[28] X. Chen, M. . McElroy, and C. Kang, “Integrated Energy Systems for Higher Wind Penetration in China: Formulation, Implementation and Impacts,” *IEEE Trans. Power Syst.*, pp. 1–1, 2017, doi: 10.1109/TPWRS.2017.2736943.

[29] Z. Li and Y. Xu, “Optimal coordinated energy dispatch of a multi-energy microgrid in grid-connected and islanded modes,” *Appl. Energy*, vol. 210, pp. 974–986, Jan. 2018, doi: 10.1016/j.apenergy.2017.08.197.

[30] J. Bartram, Ed., *Legionella and the prevention of legionellosis*. Geneva: World Health Organization, 2007.

[31] G. Incandela, “Simulazione di un sistema solare termico per produzione di acqua calda sanitaria e riscaldamento di un’abitazione,” Università degli Studi di Padova, 2015.

[32] W. Gu, J. Wang, S. Lu, Z. Luo, and C. Wu, “Optimal operation for integrated energy system considering thermal inertia of district heating network and buildings,” *Appl. Energy*, vol. 199, pp. 234–246, Aug. 2017, doi: 10.1016/j.apenergy.2017.05.004.

[33] S. A. Kalogirou, “Solar Space Heating and Cooling,” p. 75.

[34] “Domestic water heating - Energy Education.” https://energyeducation.ca/encyclopedia/Domestic_water_heating (accessed Feb. 28, 2020).

[35] Y. Xing, A. agdanavicius, S. Lannon, M. Pirouti, and T. asset t, “LOW TEMPERATURE DISTRICT HEATING NEWTORK PLANNING WITH FOCUS ON DISTRIBUTION ENERGY LOSSES,” p. 10, 01 .

[36] A. Anvari-Moghaddam and A. Rahimi-Kian, “Optimal Smart Home Energy Management Considering Energy Saving and a Comfortable Lifestyle,” *IEEE Trans. SMART GRID*, vol. 6, no. 1, p. 9, 2015.

[37] R. T. Rockafellar, *Optimization Under Uncertainty*. University of Washington, 2001.

[38] “Stochastic Programming | GAMS.” https://www.gams.com/latest/docs/UG_EMP_SP.html (accessed Mar. 27, 2020).

[39] “Stochastic Linear Programming | NEOS.” https://neos-guide.org/content/Stochastic-Linear-Programming.

[40] C. Zhang, Y. Xu, Z. Y. Dong, and L. Yang, “Multi-Timescale Coordinated Adaptive Robust Operation for Industrial Multi-Energy Micro-Grids with Load Allocation,” *IEEE Trans. Ind. Inform.*, pp. 1–1, 2019, doi: 10.1109/TII.2019.2907710.

[41] Y. An and . Zeng, “Exploring the Modeling Capacity of Two-Stage Robust Optimization: Variants of Robust Unit Commitment Model,” *IEEE Trans. Power Syst.*, vol. 30, no. 1, pp. 109–122, Jan. 2015, doi: 10.1109/TPWRS.2014.2320880.

[42] D. Bertsimas, D. B. Brown, and C. Caramanis, “Theory and Applications of Robust Optimization,” *SIAM Rev.*, vol. 53, no. 3, pp. 464–501, Jan. 2011, doi: 10.1137/080734510.

[43] J. rownlee, “A Gentle Introduction to Monte Carlo Sampling for Probability,” *Machine Learning Mastery*, Nov. 03, 2019. https://machinelearningmastery.com/monte-carlo-sampling-for-probability/ (accessed Mar. 28, 2020).

[44] L. Wu, M. Shahidehpour, and T. Li, “Stochastic Security-Constrained Unit Commitment,” *IEEE Trans. Power Syst.*, vol. 22, no. 2, pp. 800–811, May 2007, doi: 10.1109/TPWRS.2007.894843.

[45] J. Lofberg, “YALMIP: A toolbox for modeling and optimization in MATLA ,” in *2004 IEEE international conference on robotics and automation (IEEE Cat. No. 04CH37508)*, 2004, pp. 284–289.
[46] “Gurobi - The fastest solver,” *Gurobi*. https://www.gurobi.com/.
[47] A. K. asu , S. Chowdhury, and S. P. Chowdhury, “Impact of Strategic Deployment of CHP- ased DERs on Microgrid Reliability,” *IEEE Trans. Power Deliv.*, vol. 25, no. 3, pp. 1697–1705, Jul. 2010, doi: 10.1109/TPWRD.2010.2047121.
[48] “JRC Photovoltaic Geographical Information System PVGIS - European Commission.” https://re.jrc.ec.europa.eu/pvg_tools/en/tools.html#MR.
[49] “Dati Esercizio - Terna spa.” https://www.terna.it/it/sistema-elettrico/dispacciamento/dati-esercizio#datiGiornalieri.
[50] “Lampedusa e Linosa, Italy Weather Conditions | Weather Underground.” https://www.wunderground.com/weather/it/lampedusa-e-linosa/35.50,12.61.